Lactate Detection Using Non-Enzymatic Catalytic Materials

by

Mohamed Okasha

A thesis

presented to the University of Waterloo

in fulfilment of the

thesis requirement for the degree of

Master of Science

in

Chemistry (Nanotechnology)

Waterloo, Ontario, Canada, 2022

Author’s Declaration

I hereby declare that I am the sole author of this thesis. This is a true copy of the thesis, including any required final revisions, as accepted by my examiners.

I understand that my thesis may be made electronically available to the public.

Abstract

An Anastomotic leak (AL) can be defined as the leakage of gastrointestinal fluids into the abdominal cavity at the site of an anastomosis. It is a post-operative complication that affects thousands of patients annually presenting a mortality rate that ranges between 10-15%. Lactate, the conjugate base of lactic acid (LA) is a by-product formed from anaerobic respiration and therefore possesses the potential to be used in the detection of ischemia and ALs if monitored post-surgery. NERv technology Inc., has developed a device aimed at detecting complications post-surgery, with the aim to potentially detect ALs more accurately. The device attaches inline onto surgical drains that are attached post-surgery to drain excess fluid from the abdominal cavity. This device contains micron sized sensors that offer continuous monitoring of the effluent luminal fluid. However, to better detect ischemia in patients and increase likelihood of AL detection, a non-enzymatic catalytic LA sensor is researched and developed with the objective of continuously monitoring LA in isotonic pH conditions. Current LA sensing relies on enzymatic detection, using enzymes such as lactate oxidase (LOD) and lactate dehydrogenase (LDH), which are specific but suffer in terms of stability due to enzyme degradation and denaturation. Current LA detection using non-enzymatic catalytic metals and/or metal oxides can only detect LA through oxidation in either highly acidic or basic media, and although metal and/or metal oxide sensors are theoretically superior to enzymatic sensors, they often fall behind in terms of selectivity. In this work, it is demonstrated that LA detection in isotonic pH can be achieved by using a combination of Pt metal and Ni oxide as a catalyst and co-catalyst in the form of self-assembled nanocomposite chains achieved through the aid of citrate capped gold nanoparticles (AuNP). The nanocomposite comprised of a Au NP core, with a metallic Pt shell and domains of oxidized Ni surrounding the core. The nanocomposite was able to detect positive and negative changes in LA concentrations

in real-time in a PBS buffer with decent selectivity and linearity. The nature of the nanocomposite chains can also potentially allow it to be fabricated into a small sensor size, making it theoretically possible to integrate into NERv's device with further optimization.

Acknowledgements

I would like to start by thanking my supervisor Dr. Vivek Maheshwari for the phenomenal support and guidance throughout this thesis research and defence as well as for facilitating the research and technology that will enable the creation of a new generation of future sensors that can be used in many applications. His direction, vision and input are deeply appreciated by me and every party involved in this project. I would also like to thank my supervising committee Dr. Juewen Liu and Dr. Pavle Radovanovic for agreeing to oversee this project and for their time and efforts. I am also extremely thankful for my lab members Hua Fan, Avi Mathur and Saikiran Khamgaonkar for providing me with tremendous help, support and teaching that enabled me to complete my work for this thesis. I greatly appreciate their guidance and presence that creates a friendly environment for anyone in the lab. I would also like to thank NERv Technologies and Youssef Helwa, Abdallah Elfalou, Amr Abdelgawad and Ricky Tjandra for their tremendous support throughout. I am also extremely thankful to the Mitacs organization and their committee that saw the potential value in this project and agreed to financially support it. I would also like to extend a thank you to the University of Waterloo's Chemistry department, Waterloo's Institute of Nanotechnology, and office of research for their support in the enablement and creation of this research. I am also enormously thankful for my parents, family, and friends for their motivation, help and moral support that encouraged me to work hard and pursue this research. I extend my thankfulness and gratitude to everyone involved for enabling me to work on this proposal for whom without this would not have been possible, and I thank God for providing me with their support and enabling such opportunities and blessing.

Table of Contents

Author's Declaration ii

Abstract iii

Acknowledgements v

List of Figures viii

List of Abbreviations xii

Chapter 1: Background and Introduction 1

Anastomotic Leaks and Methods of Detection 1

Detecting Anastomotic Leaks Using Lactic Acid 3

Sensor Requirements 6

Enzymatic vs Non-Enzymatic Lactic Acid Detection 7

Using AuNP Self-Assembled Nanocomposite Chains 10

Current Non-enzymatic Catalysts for Lactic Acid Detection 16

Chapter 2: Nanocomposite Characterization 18

Synthesizing Ni & Pt nanocomposite chains using AuNP self-assembly 18

Microscopic Characterization of the Au Nanocomposite Chains 19

X-Ray Photoelectron Spectroscopy (XPS) of the AuNP Composite Chains 22

Chapter 3: Nanocomposites Lactate Sensing 29

Validating LA Oxidation Capability Using Pt & Ni AuNP Nanocomposite Chains ... 29

Testing Pt & Ni AuNP Nanocomposite Chains in Isotonic pH Conditions 31

Ni Pt Pre-assembled Nanocomposite Chain LA Sensitivity..... 32

Testing LA Specificity and Hysteresis 37

LA Detection Conclusion 40

Proposed Reaction Mechanism..... 41

Chapter 4: Conclusions and Future Work..... 44

Using AuNP Nanocomposite Chains For LA Detection Summary and Conclusions .. 44

Future Work and Optimization..... 44

References..... 47

Appendix..... 55

List of Figures

Figure 1-1: NERv's device attached inline to surgical drains to monitor fluid drained from the peritoneal cavity in real-time. 2

Figure 1-2: The chemical structure of lactic acid. 4

Figure 1-3: General reaction mechanism for non-enzymatic lactate catalysis. From Ref 23. 9

Figure 1-4: TEM images of (a) assembled Pt^{4+} on Au NP chains, (b) reduced Pt and Au nanocomposites, (c) high resolution TEM and (d) EELS elemental mapping of the reduced chain structures. From Ref 27. 11

Figure 1-5: Demonstration of Au NP chain self-assembly. From Ref 27. 12

Figure 1-6: NP composite self-assembly process using (a) pre-assembled chains to create a product with segregated domains and (b) using a mixed ion solution to create a product with a homogenous distribution of compounds. From Ref 27. 13

Figure 1-7: TEM image of (a) mixed pre-assembled chains of reduced Pt and Ru on Au NP chains where regions of Pt is circled in blue and Ru in red, (b) EELS elemental mapping of the chain structure, (c) TEM of the chains formed from the mixed ions showing homogenous distribution, and (d) EELS elemental mapping of the chain structures. From Ref 27. 14

Figure 1-8: Graphs show a (a) CV curve of lactate solutions of different concentrations in 0.5M H_2SO_4 oxidised on a Pt electrode and (b) the plotted anodic currents vs lactate concentrations at an oxidation potential of 1.35V. From Ref 23. 15

Figure 1-9: Graphs showing CV curves of lactate solutions of different concentrations in 0.2M NaOH and 0.2M KCl oxidised on a (a) NiO electrode and (b) $Ni(OH)_2$ electrode. The plotted anodic currents vs lactate concentrations at an oxidation potential of 0.5V for (c) NiO and (d) $Ni(OH)_2$. From Ref 24. 15

Figure 2-1: SEM image of AuNP pre-assembled nanocomposite chains comprised of 1:2 Ni: Pt. 20

Figure 2-2: HRTEM image of (a) 1:2 Ni:Pt AuNP pre-assembled nanocomposite chains, Ni domains circled in red, and (b) EELS elemental mapping of the chains structure. 21

Figure 2-3: EELS elemental mapping of 1:10 Ni:Pt AuNP pre-assembled nanocomposite chains. 22

Figure 2-4: High-resolution XPS of the Ni2p spectra for 1:10 & 1:2 Ni:Pt AuNP pre-assembled nanocomposite chains. 23

Figure 2-5: High-resolution XPS of the Ni2p spectra for Au Ni reduced, Au Ni with NaOH only and Au Ni with NaOH and H_2O_2 pre-assembled nanocomposite chains..... 25

Figure 2-6: High-resolution XPS of the Pt4f spectra for 1:10 & 1:2 Ni:Pt AuNP pre-assembled nanocomposite chains. 26

Figure 2-7: High-resolution XPS of the Au4f spectra for 1:2 Ni:Pt AuNP pre-assembled nanocomposite chains. 27

Figure 3-1: CV curve of Pt AuNP self-assembled chains in different LA concentrations in 0.5M H_2SO_4 (a). The plotted anodic currents vs lactate concentrations at an oxidation potential of 1.4V (b), and CV cycle close-up (c). 29

Figure 3-2: CV curve of Ni AuNP self-assembled chains in different LA concentrations in 0.2M NaOH and 0.2M KCl (a). The plotted anodic currents vs lactate concentrations at an oxidation potential of 0.46V (b), and CV cycle close-up (c). 30

Figure 3-3: Real-time LA detection using CA at an oxidation potential of 1.44V vs SCE for Ni AuNP nanocomposite chains in a 2X PBS solution. Each vertical line shows LA addition. 32

Figure 3-4: The plotted anodic currents vs lactate concentrations at an oxidation potential of 1.5V vs SCE for 1:2 Ni:Pt (a) and 1:10 Ni:Pt (b) oxidised and reduced pre-assembled AuNP nanocomposite chains in a 2X PBS solution. Insets are their respective second CV cycles in all plotted lactate concentrations. 33

Figure 3-5: Real-time LA detection using CA at an oxidation potential of 1.44V vs SCE for 1:2 Ni:Pt oxidised and reduced pre-assembled AuNP nanocomposite chains in a 2X PBS solution. 35

Figure 3-6: A close-up look at the real-time LA detection using CA at an oxidation potential of 1.44V vs SCE for 1:2 Ni:Pt oxidised and reduced pre-assembled AuNP nanocomposite chains in a 2X PBS solution. Each graph represents an event when LA was added to the system. 36

Figure 3-7: The plotted relative sensitivities of lactate, glucose and acetic acid at an oxidation potential of 1.5V vs SCE for 1:10 Ni:Pt oxidised and reduced pre-assembled AuNP nanocomposite chains in a 2X PBS buffer. 37

Figure 3-8: The plotted hysteresis for lactate at an oxidation potential of 1.5V vs SCE for 1:2 Ni:Pt oxidised and reduced pre-assembled AuNP nanocomposite chains in a 2X PBS solvent..... 39

Figure 3-9: Real-time LA detection with decreasing LA concentration using CA at an oxidation potential of 1.44V vs SCE for 1:2 Ni:Pt oxidised and reduced pre-assembled AuNP nanocomposite chains in a 2X PBS solution..... 40

Figure S-1: SEM image of AuNP pre-assembled nanocomposite chains comprised of 1:10 Ni: Pt. SEM shows similar structure to 1:2 Ni:Pt nanocomposite. 55

Figure S-2: XRD pattern of AuNPs, reduced Ni AuNPs, reduced Pt AuNPs, and reduced 1:3 Ni:Pt AuNP nanocomposite chains. Pt peaks are labelled as well as Au (111). Ni did not show peaks implying it is amorphous. 56

List of Abbreviations

AL	Anastomotic Leak
ATP	Adenosine Tri Phosphate
AuNP	Gold Nanoparticles
CA	Chronoamperometry
CV	Cyclic Voltammetry
EDL	Electrical Double Layer
EELS	Electron Energy Loss Spectroscopy
FSEM	Field Emission Scanning Electron Microscopy
GCE	Glassy Carbon Electrode
HRTEM	High Resolution Transmission Electron Microscopy
LA	Lactic Acid
LDH	Lactate Dehydrogenase
LOD	Lactate Oxidase
NP	Nanoparticle
OER	Oxygen Evolution Reaction
PBS	Phosphate Buffered Saline
SCE	Saturated Calomel electrode
SEM	Scanning Electron Microscopy
SPR	Surface-Plasmon Resonance
TCA	Tricarboxylic Acid Cycle

TEM	Transmission Electron Microscopy
TRL	Technology Readiness Level
UV-viz	Ultraviolet Visual Spectroscopy
WE	Working Electrode
XPS	X-ray Photoelectron Spectroscopy
XRD	X-ray Diffraction

Chapter 1: Background and Introduction

Anastomotic Leaks and Methods of Detection

Serious surgical complications can significantly contribute to the stress levels of hospital staff.[1] Even after an operation, surgeons worry about their patients' health as there is usually an associated risk of developing a post-operative complication. The incidence rate of developing a complication post-surgery can be as high as 15% in patients undergoing surgery.[2,3] In many cases, if these complications are not identified and treated in a timely manner, patient mortality rate significantly increases.[4] One of the most common and dreaded post-operative complications in general surgery is an anastomotic leak (AL).[4,5] An AL can be defined as the leakage of abdominal or gastrointestinal fluids at the site of an anastomosis.[6] An anastomosis is a surgical connection between organs, typically tubular organs such as intestines, where the surgeon connects or reconnects parts of the organs after surgery. When gastrointestinal fluid leaks through the anastomosis performed during surgery into the peritoneum or abdominal cavity surrounding the organ, this is referred to as an AL. Affecting thousands of patients annually, with a mortality ranging between 10% to 15%, ALs are also feared as they have the potential to trigger a cascade of other life-threatening complications such as peritonitis and sepsis.[7] The incidence timeline for ALs can be as soon as several hours post-surgery or up to several days or longer, thus requiring frequent monitoring and checkups from hospital staff.[8]

Presently, the gold standard for the detection of ALs and other post-operative complications rely on frequent nurse checkups as well as blood tests and imaging methods such as CT scans and MRIs during hospitalization, which are infrequent in their monitoring and don't always produce effective results and diagnosis in a timely manner. Furthermore, they can also add

unnecessary costs during the hospital stay to an already costly bill, especially if no complications transpire.[8] It is agreed that one of the key methods to decreasing or preventing mortality caused by ALs is the early intervention and treatment of this complication.

Recent advances in sensing technologies have allowed the development of miniaturized, portable, stable, and less costly sensors with potential uses in many applications including the medical field with minimal biofouling. Research has found that monitoring certain key analytes in the body can help predict the prevalence of ALs. An example is the monitoring of peritoneal pH, certain cytokines as well as lactate to help identify ALs earlier than the current gold standard, potentially allowing for quicker intervention and potentially reducing hospital costs by eliminating unnecessary tests and surgical interventions from late AL detection. NERv technology Inc., is a biomedical device start-up working on technology to detect ALs quicker than the gold standard. This is achieved through the development of a miniature sensing platform technology designed to monitor the effluent fluid in patients' peritoneal drains in real-time. The aim is to detect ALs as

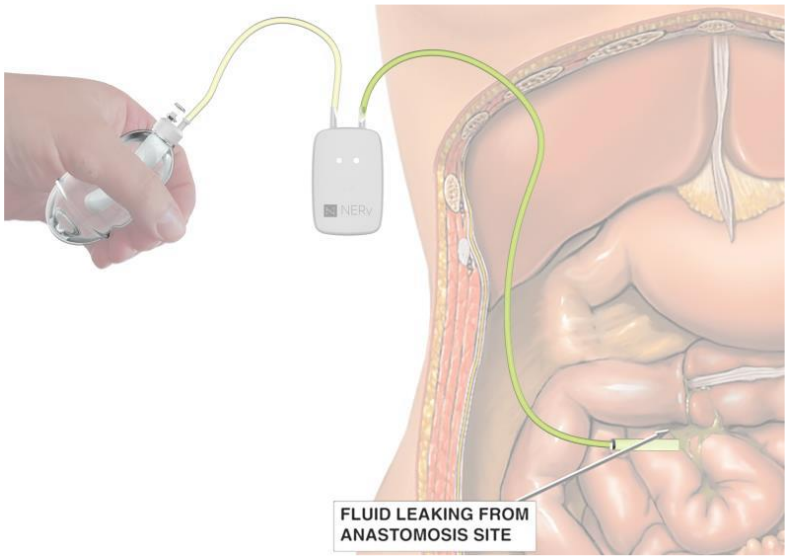

Figure 1-1: NERv's device attached inline to surgical drains to monitor fluid drained from the peritoneal cavity in real-time.

soon as they occur by monitoring chemical and physiological changes in real time such as changes in pH, ionic conductivity, and temperature.

As observed in Figure 1-1, the medical device attaches inline to a surgical drain that the surgeon places near the anastomotic site. The surgical drain is usually placed by surgeons at the end of a surgical procedure to drain out excess fluids that are formed during recovery. In the event of an AL, fluid leaks into the peritoneal cavity surrounding the organ tissue but is then drained through the attached drain and ends up passing by NERv's sensor platform where the effluent is monitored continuously in real-time for changes in pH, conductivity and temperature. An AL can trigger a change in the peritoneal fluid's pH and ionic conductivity levels as the gastrointestinal pH and ionic concentration differs from that of the peritoneal fluid in the abdominal cavity as both fluids mix when the gastrointestinal fluids leak into the peritoneum.[9]

Detecting Anastomotic Leaks Using Lactic Acid

Unfortunately, in many instances, monitoring a single analyte or chemical change can be insufficient on its own. Monitoring and observing trends in multiple key analytes can significantly increase the positive predictive value and decrease false positive readings of ALs. Thus, the addition of a new sensor to NERv's sensing platform can potentially increase its efficacy in AL detection. The proposed additional analyte to be detected is lactate, or lactic acid (LA).

Lactate, a hydroxy monocarboxylic acid anion, is the conjugate base of LA (Figure 1-2). In biology, it is primarily known as a by-product of anaerobic respiration; this is when cells consume glucose in order to produce energy, but not enough oxygen is available to undergo the traditional aerobic respiration mechanism and the reaction cannot be driven to completion.[10] Traditionally, cells undergo metabolism to produce energy in the form of Adenosine Tri Phosphate

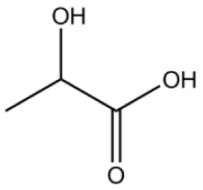

Lactic Acid

Figure 1-2: The chemical structure of lactic acid.

(ATP) by breaking down glucose. In this process, pyruvate is produced as a by-product in addition to NADH and H^+ from NAD+ that acts as the oxidizing agent in a process called glycolysis.[10] It is the presence of oxygen that drives aerobic respiration as it allows the produced pyruvate to pass through the Tricarboxylic acid (TCA) cycle in order to produce more ATP energy and also producing carbon dioxide as a by-product. As this is only achieved in the presence of a sufficient oxygen supply in cells, when not enough oxygen is present, the metabolic pathway diverges at this step in a process called anaerobic respiration. As the pyruvate by-product cannot go through the TCA cycle, it alternatively undergoes fermentation so that it can restore the NAD+ consumed during glycolysis. This process, referred to as fermentation, is what produces LA, and since the accumulation of LA in the body is harmful, the liver ends up further metabolizing it to get rid of it.

The significance of using LA as a potential early marker of ALs is due to it being a primary marker of ischemia. Ischemia is a medical condition that occurs when there is an inadequate blood supply reaching organ tissues, and following abdominal surgery, there is an increased risk of developing ischemia.[11] After organ tissues are stitched by the surgeon at the anastomosis, there is a possibility that the blood supply to the surrounding tissue becomes obstructed leading to the decrease in oxygen supply and hence the need to undergo anaerobic respiration by those organ tissues leading to the production of LA. The produced LA starts accumulating at the anastomotic site as well as diffusing out into the abdominal or peritoneal cavity and mixing in with the

peritoneal fluid which is what allows its potential detection. Consequently, the accumulation of LA at the ischemic site causes the intracellular pH levels to decrease. These acidic conditions render ATP-ase dependent ion transport mechanisms obsolete, which in turn leads to a build up of calcium inside the cells causing them to rupture and die by necrosis.[12] It is the death of the ischemic organ tissue at the anastomotic site which causes the luminal fluid passing through the organ to leak into the abdominal cavity, hence the onset of an AL event. The weakened abdominal wall due to ischemia increases the risk of ALs, making ischemia detection a potential method for early AL detection, and the primary method of detecting ischemia is through LA measurements.

In addition to the causation effect, research has also shown a correlation between the diagnosis of ALs in patients and elevated levels of LA in the peritoneum as well as in blood, or serum post-surgery.[12] The risk of surgical reintervention due to AL was found to significantly correlate to a peritoneal LA level greater than 9.1mmol/L more so when the peritoneal-serum ratio was greater than 4.5. Additionally, LA in the peritoneum was found to respond faster to changes than in serum, making it a suitable marker for AL detection. Moreover, not only is LA useful in AL detection, but it can also be used as an indicator for other types of bowel ischemia and even sepsis in some cases. Physicians have been using blood LA as a marker for general health, as its buildup can lead to many unwanted conditions such as metabolic acidosis, and an abnormal LA concentration has been associated with several unwanted conditions in general.[13] Athletes have also been using it as a marker for athletic performance by measuring LA in sweat, as it acts as an indicator for oxygen availability to cells and helps evaluate their endurance and performance.[14,15] Furthermore, hyperlactemia, defined as being a slight and persistent elevation of lactate ranges from around 2-4mM, and persistent lactate levels greater than 4mM in serum can be potentially diagnosed as lactic acidosis.[18] Although these standards are from serum lactate levels, the values

translate very closely to peritoneal lactate levels.[12] This in turn makes LA a valuable marker and target for detection in the medical field, and introduces the need for next generation sensing technologies with enough stability, portability, sensitivity and specificity to be beneficial to future medical technologies and applications.

This thesis takes a step in the creation of such technology. Ultimately the aim is to create a senor that is capable of continuous accurate monitoring of LA in biological conditions in real time in order for it to be of use in the early detection of ALs.

Sensor Requirements

Such a sensor has varying requirements to make it effective for its application. For once, it needs to be specific to the analyte of interest, meaning the sensor should only respond to changes triggered by a change in LA concentration, and not any other analyte. The sensor needs to be sensitive enough in its detection in order to differentiate between changes in LA concentration and has to be accurate enough to reproduce a similar output each time the same concentration is measured. Such a sensor would also need to be stable for the duration of time needed for it to perform its function and have at least a somewhat linear correlation between sensor output and LA concentration to more accurately map changes in sensor output to the measured LA and to make the calibration process simpler. Furthermore, in order to fit into NERv's sensing platform, the sensor would need to be small in size, occupying a maximum area of 10mm x 10mm x 500µm.

The normal range of lactate is between 0.5-1.5mM, and elevated levels have been found to exceed 7mM during ischemic events.[16,17] And since peritoneal LA greater than 9.1mM is greatly correlated to ALs, the sensor should be able to detect LA in the range of at least 1mM up to 9mM with a minimum sensitivity of 0.5mM. The sensor would also need to be operational at isotonic

conditions and pH levels such as that of the peritoneal fluid's which ranges between 7.6-7.8.[19] However, one of the biggest challenges in creating sensors for biomedical applications is shelf-life, stability during operation as well as susceptibility to biofouling. An important requirement for this sensor is stability, and this has been hard to achieve using enzymatic LA sensors, which are the most common sensor type as well as the only commercially available solution.

Enzymatic vs Non-Enzymatic Lactic Acid Detection

Enzymatic LA sensing approaches are predominant in both literature as well as commercial availability. They primarily use lactate oxidase (LOD) or lactate dehydrogenase (LDH) as enzymes to catalyze the conversion of LA to pyruvate. LOD catalyzes lactate oxidation in the presence of dissolved oxygen to form pyruvate as well as hydrogen peroxide. In LOD based sensors, the electrochemically active hydrogen peroxide is reduced at the electrode to produce a current that is proportional to the concentration of lactate in solution.[20,21]

$$Lactate + O_2 \xrightarrow{LOD} Pyruvate + H_2O_2 \quad (1\text{-}1)$$

$$H_2O_2 \rightarrow O_2 + 2H^+ + 2e^- \quad (1\text{-}2)$$

The need for oxygen in solution for the LOD catalysis can affect the sensor's detection limits. Thus, many other enzymatic LA sensors utilize LDH enzymes. LDH is highly catalytic and also converts LA to pyruvate but using a different pathway. Using NAD+ as a coenzyme, LDH converts lactate and NAD+ to pyruvate, NADH and protons. NADH is then further oxidised due to the applied potential of the electrodes back to NAD+ producing a detectable oxidation current that is proportional to the lactate concentration in solution.[20]

$$Lactate + NAD^+ \xrightarrow{LDH} Pyruvate + NADH + H^+ \quad (1\text{-}3)$$

$$NADH \rightarrow NAD^+ + H^+ + 2e^- \quad (1\text{-}4)$$

Both of these enzymatic approaches produce sensors that are very specific to LA, which is one of the main reasons for their use. The enzymes can be functionalized onto electrodes which can be done using a variety of different methods ranging from simple adsorption to the use of linkers to create covalent bonds between the electrode surface and the enzyme.[22] Overall, this method of lactate detection is the most common to date due to its highly specific nature, as well as its ability to detect LA in biological conditions, however, it still possesses many limitations.[20]

The main issue with enzymatic approaches is the limited stability and operating conditions the sensor can withstand during storage and operation. Although enzyme-based sensors have come a long way in terms of stability through the use of stabilizing agents and manufacturing improvements over time, they still suffer fragility challenges due to denaturation and natural degradation of the enzymes over time.[20,22] Since a primary requirement of the LA sensor is long term stability, this means that using enzymatic approaches is suboptimal for this application. In order to combat this issue, non-enzymatic LA sensing methodologies have been examined. Such approaches rely on catalytic metals and metal oxide materials to oxidise LA allowing for their potential use as sensors. Some research has shown that LA sensing can be achieved using catalysts such as platinum, nickel oxide and nickel hydroxide.[23,24,25] The use of metals and metal oxides can potentially allow for the development of more stable sensors compared to their enzymatic counterparts, allowing them to be used for longer periods of time making them more suitable for NERv's application.

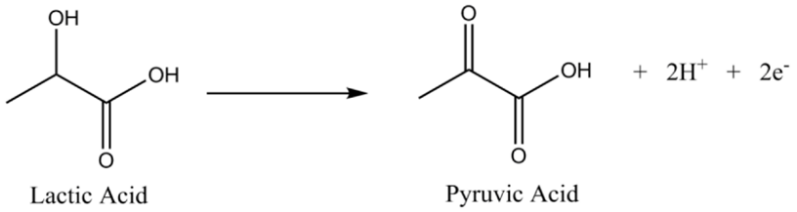

Figure 1-3: General reaction mechanism for non-enzymatic lactate catalysis. From Ref 23.

The products produced from LA catalysis using Pt in literature is similar to that of NiO and $Ni(OH)_2$. LA contains a hydroxyl group similar to that of alcohols which is targeted by these metals and metal oxides. The catalytic metal or metal oxide oxidises the secondary hydroxyl group of LA to form pyruvate, protons and free electrons which are transferred to the electrode and detected as a change in oxidation current signal (Figure 1-3).[23,25] There will probably be variation in the reaction mechanism between these inorganic catalysts and LA, which has still not been studied, but the end result remains similar. Such sensors have reported sensitivities and ranges within NERv's desired sensor specification, and hypothetically, should outperform the enzymatic counterparts in terms of stability and longevity as metals do not denature like proteins, although these sensors have yet to undergo extensive testing for their stability performance in literature.

The forementioned catalytic metal and metal oxide sensors however still require a lot of optimization and still possess several limitations. For once, it is theorized, but is not yet confirmed that these metal and metal oxide/hydroxide sensors would increase the stability of the proposed sensor as none of the reported sensors have been examined for extended lifetime by continuous testing. Furthermore, a catalyst such as Pt for example, can only oxidise LA in extremely acidic pH conditions, and NiO and $Ni(OH)_2$ are only capable of oxidising LA in extremely basic conditions. This is a common metal and metal oxide catalyst limitation also found in catalytic fuel cells. As a requirement of the sensor is to operate in isotonic pH conditions close to neutral,

tackling this challenge will be addressed in this thesis. Catalyst poisoning is also a potential problem when it comes to inorganic metal catalysts, but such an issue can sometimes be overcome through the use of a suitable co-catalyst.[26] Moreover, the tertiary structure of enzymes allows them to be very specific to their target analyte. As this isn't the case for non-enzymatic sensors, the aspect of specificity can sometimes pose as a potential challenge to be overcome. Although in literature, Pt and $NiO/Ni(OH)_2$ have shown some specificity to LA, they haven't been thoroughly tested on similarly structured molecules and alcohols.

The primary objective of this thesis is to find a suitable metal and/or metal oxide catalyst and co-catalyst that is capable of continuous detection of LA in isotonic pH conditions with good specificity, and that has been demonstrated in the work of this thesis through a combination of Pt and $NiO/Ni(OH)_2$ as a catalyst/co-catalyst system fabricated using self-assembled gold nanoparticle chains.

Using AuNP Self-Assembled Nanocomposite Chains

Most literature utilizing a metal or metal oxide as a catalyst have either used them in their bulk metallic structure or in a powder form. As a requirement of this sensor is to be as small as possible, the catalyst used is in nanoparticle (NP) form. This is achieved through a technique developed by the Maheshwari group, using citrate capped gold NPs that can self-assemble in the presence of metal cations to form micron-long chain structures, with the metal forming a shell around the gold NPs.[27] The example shown in Figure 1-4 is that of Au NP mediated self-assembly of platinum. The images show high resolution transmission electron microscopy (TEM) of Pt^{4+} cations that have been self assembled using Au NPs and reduced to transform to Pt metal. Figure 1-4a is the image before Pt^{4+} reduction and Figure 1-4b is the image of Pt metal after reduction. Pt^{4+} can be reduced with reducing agents such as sodium borohydride ($NaBH_4$), ascorbic acid or

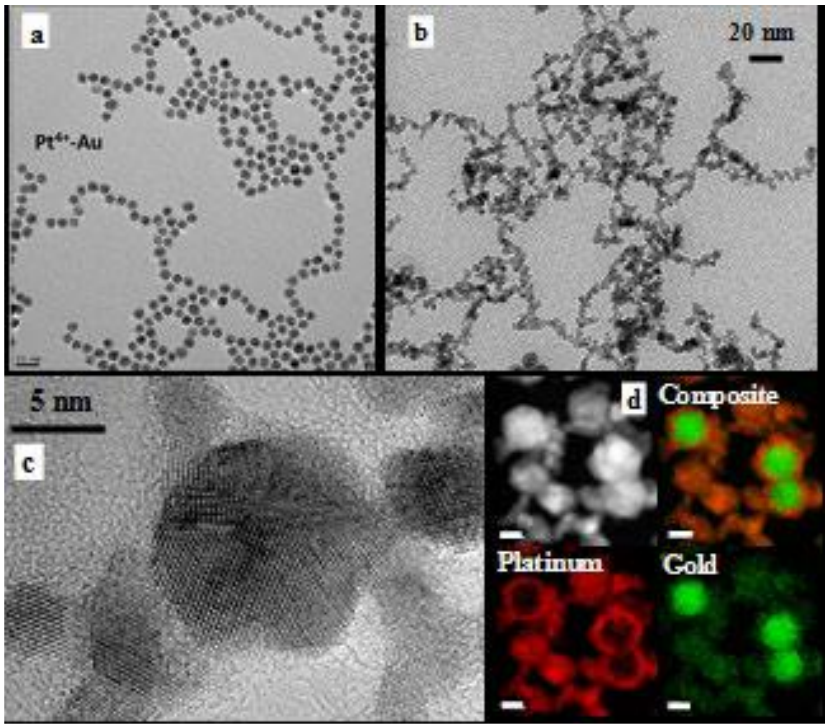

Figure 1-4: TEM images of (a) assembled Pt^{4+} on Au NP chains, (b) reduced Pt and Au nanocomposites, (c) high resolution TEM and (d) EELS elemental mapping of the reduced chain structures. From Ref 27.

other appropriate reducing agents to form metallic Pt. When reducing Pt, it can be observed that the gap between the Au NP chains is decreased leading to the formation of a continuous structure. The spacing between the NPs is decreased and are joined by the reduced metallic Pt structures to form a continuous chain network. The spacing between the NPs is assumed to be previously occupied by the Au NP citrate capping as well as the Pt^{4+} in solution. Figure 1-4c shows the shape of the spherical structure with a diameter close to 12nm, and Figure 1-4d is an electron energy loss spectroscopy (EELS) elemental mapping image of the reduced chain structure. It is observed that Pt metal formed around the Au NP chains forming a shell-like structure. Explanation of this phenomenon is that the Pt^{4+} cations are first concentrated around the negatively charged citrate capped Au NPs. Following the addition of the reducing agent, preferential nucleation of Pt occurs at the concentrated areas around the Au NP cores to form the shell-like chain structures by

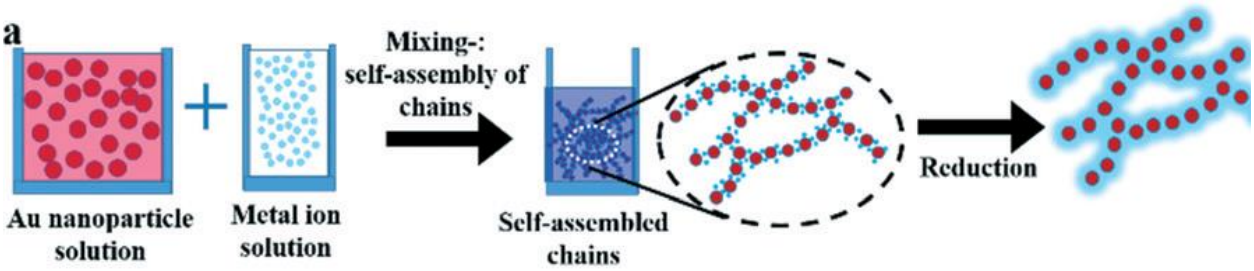

Figure 1-5: Demonstration of Au NP chain self-assembly. From Ref 27.

incorporating onto the electrical double layer (EDL) formed on the surface of the Au NPs.[27] A demonstration of this process is outlined in Figure 1-5. The salt of a metal cation such as Pt^{4+} in the form of $PtCl_4$ as an example is added to the citrate capped Au NP solution. Electrostatic forces between the positively charged Pt cation and negatively charged citrate anion leads to the formation of the self-assembled chain structure. The agglomeration of the Au NPs causes a visual change in color from red to blue, and the metal cation can then be reduced to its metallic state using a reducing agent.[27,28]

An advantage of using NP self-assembly is that it requires much fewer catalytic material to oxidise LA as opposed to the bulk catalyst. It can also be used to fabricate small sensors depending on the size of the electrode to be used. The shell-like spherical structure gives the material a high surface area for contact with the solution making it a highly effective process for this application and the reason why lesser material can be used. Platinum is an expensive metal, and the less each sensor uses, the greater the cost decrease per sensor.[25]

However, an even greater advantage of this method is the ability to combine multiple metal cations to form a hybrid combination of two or more metals or metal oxides. This is demonstrated in Figure 1-6, outlining an example of how Pt and Ru cations can be combined together during the chain self-assembly process as well as how two different methods of chain formation can affect the placement and distribution of the metal domains.[27] In Figure 1-6a, it is shown that the mixing

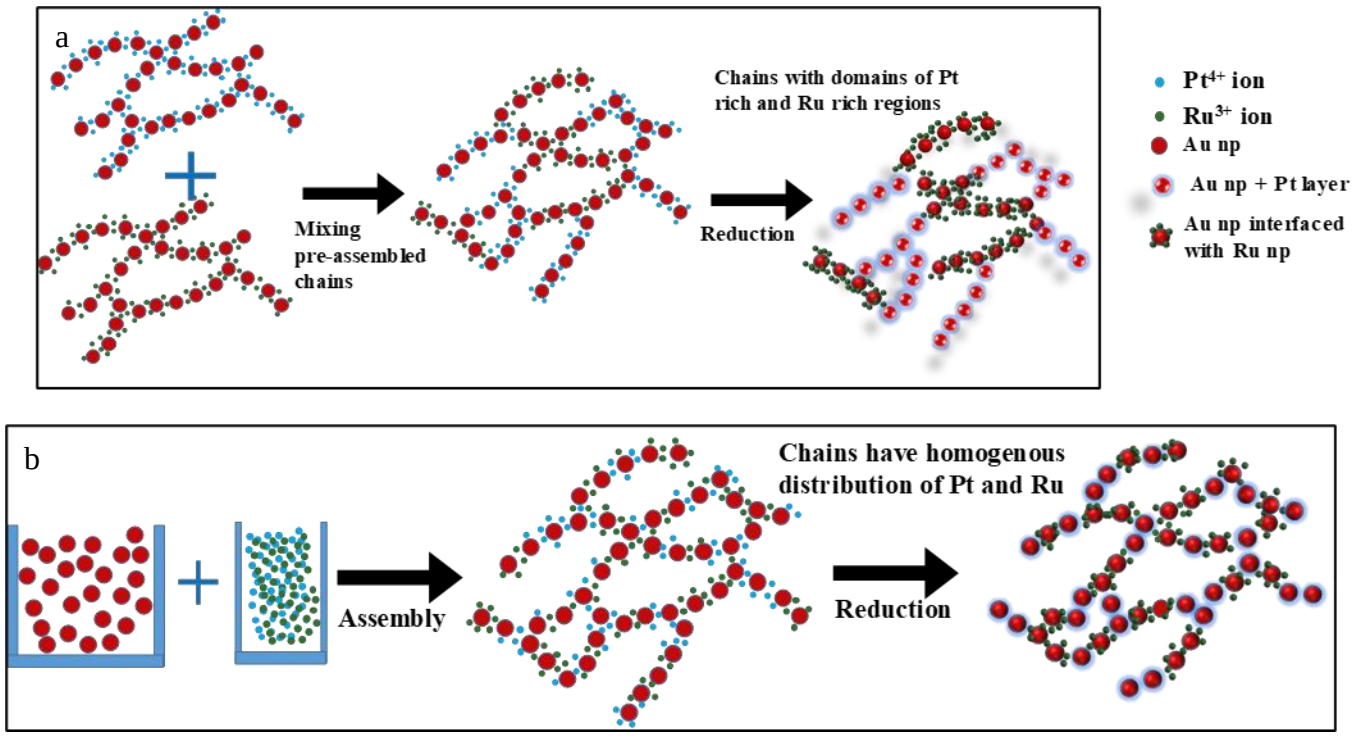

Figure 1-6: NP composite self-assembly process using (a) pre-assembled chains to create a product with segregated domains and (b) using a mixed ion solution to create a product with a homogenous distribution of compounds. From Ref 27.

two pre-assembled chains with one containing Pt and the other Ru cations, can produce chains that have distributed domains of Pt and Ru metals after reduction. In Figure 1-6b however, when the metal ions have been premixed prior to the assembly process, the formed chains after reduction would produce a homogenous distribution of both metals on the formed chain structure. Another advantage of this technique is that the amount and ratios of metals per pre-assembled chain can be controlled by adjusting the relative amounts and concentrations of cations during the pre-assembly process. The chain assembly formation time is also an important factor that can be used to control the relative domain sizes of the pre-mixed chains, as individual chain size also depends on the assembly time for the Au NPs to form the micron-long chain structures.

Figure 1-7 also shows this process. In Figure 1-7a, pre-assembled chains of Pt^{4+} and Ru^{3+} with an elemental composition of 9:1 Pt:Ru have been mixed and reduced. The TEM image shows

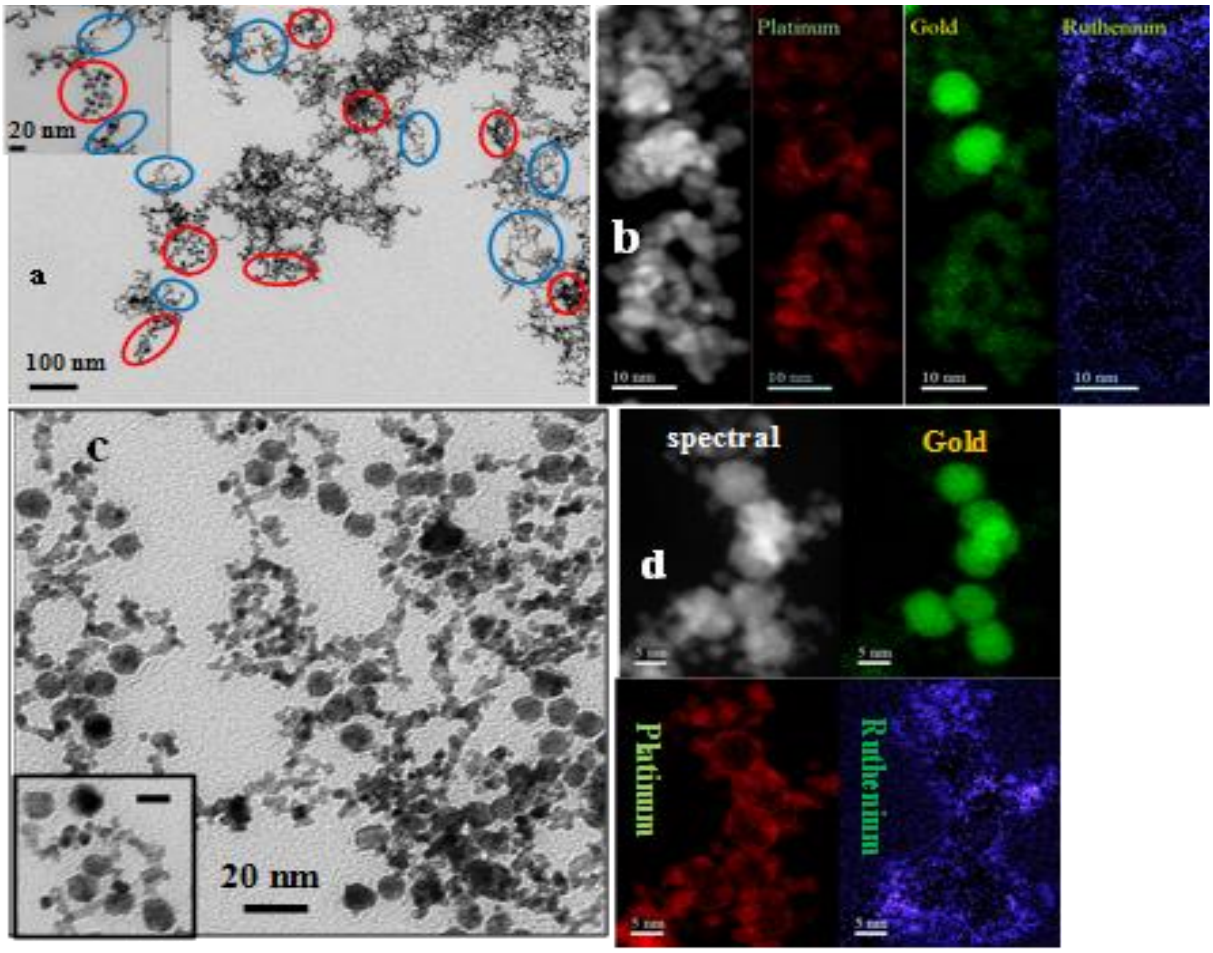

Figure 1-7: TEM image of (a) mixed pre-assembled chains of reduced Pt and Ru on Au NP chains where regions of Pt is circled in blue and Ru in red, (b) EELS elemental mapping of the chain structure, (c) TEM of the chains formed from the mixed ions showing homogenous distribution, and (d) EELS elemental mapping of the chain structures. From Ref 27.

a chain-like structure with high porosity in addition to the distinct distribution of elements by domain, where regions of Pt domain is circled in blue, and Ru in red. The domains can be identified in the images through their distinct morphologies. This is further confirmed by EELS mapping in Figure 1-7b, where more Pt is mostly present at the bottom of the image, whereas Ru is concentrated at the top. In contrast, when the metal cations are mixed beforehand, then added to the Au NPs to self-assemble into chains, then reduced, no distinct domains are visually identified as they appear to be randomly distributed. This is attributed to the homogenous distribution formed between the metals that can be observed in the TEM image in Figure 1-7c. EELS on this sample (Figure 1-7c) also further confirms this as the spatial distribution appears to be similar for both Pt

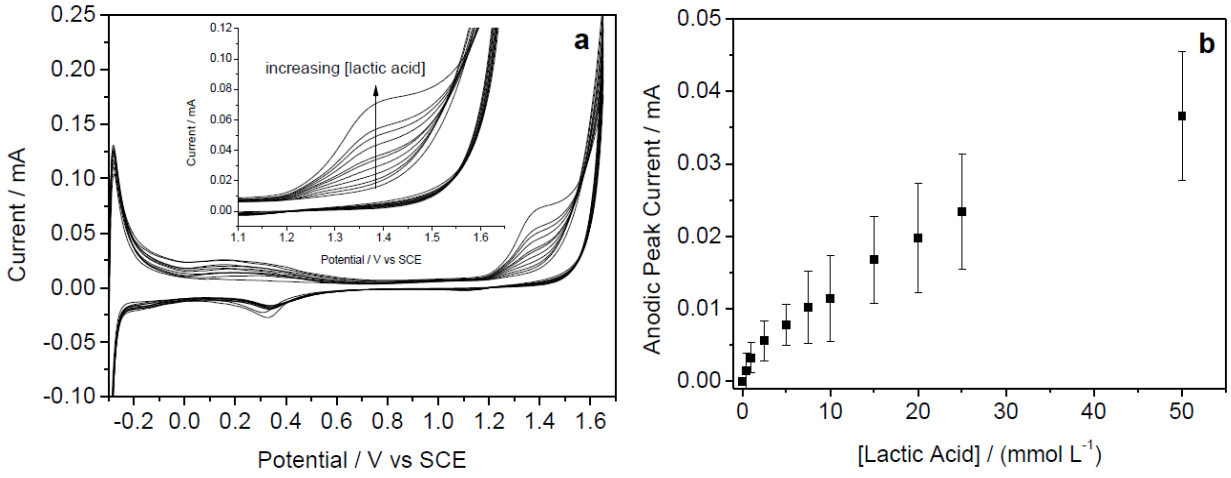

Figure 1-8: Graphs show a (a) CV curve of lactate solutions of different concentrations in 0.5M H_2SO_4 oxidised on a Pt electrode and (b) the plotted anodic currents vs lactate concentrations at an oxidation potential of 1.35V. From Ref 23.

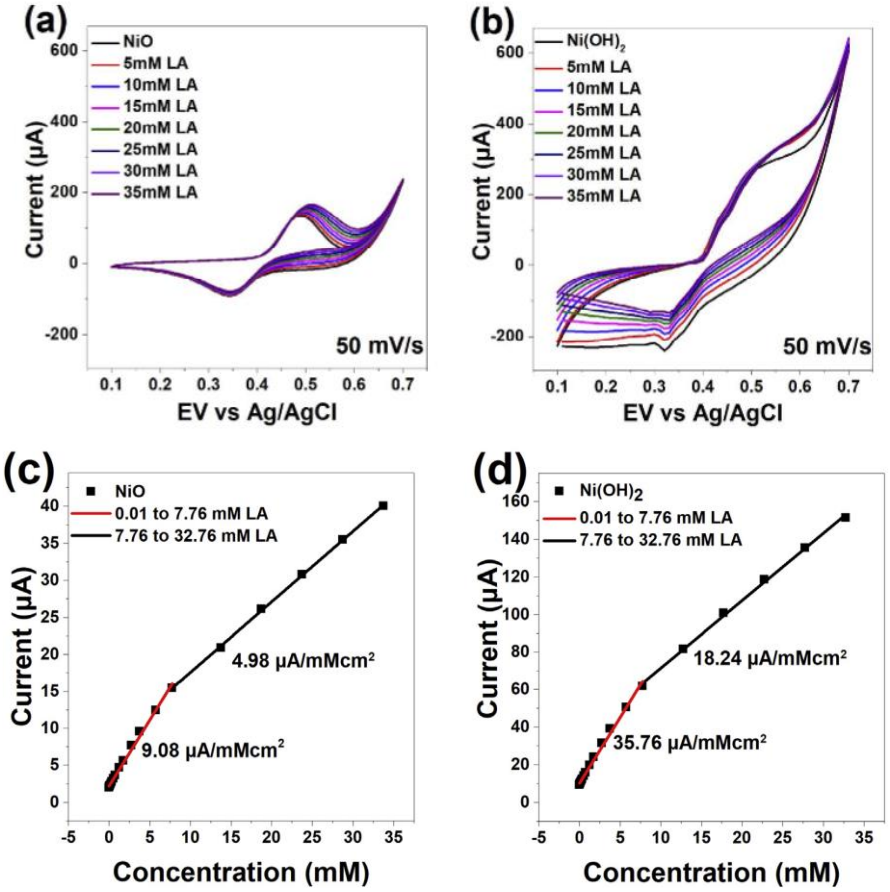

Figure 1-9: Graphs showing CV curves of lactate solutions of different concentrations in 0.2M NaOH and 0.2M KCl oxidised on a (a) NiO electrode and (b) $Ni(OH)_2$ electrode. The plotted anodic currents vs lactate concentrations at an oxidation potential of 0.5V for (c) NiO and (d) $Ni(OH)_2$. From Ref 24.

and Ru. This method is what allows the formation of the Au Pt and Au NiO/$Ni(OH)_2$ chains as a catalyst/co-catalyst system for the oxidation of LA in isotonic pH as will be discussed in this thesis.

Current Non-enzymatic Catalysts for Lactic Acid Detection

On its own, Pt metal is capable of electro-oxidising LA in extremely acidic conditions.[23] Sedenho et al. examined this by testing bulk Pt using cyclic voltammetry (CV) in different LA concentrations while observing changes in anodic current. This experiment was performed in 0.5M H_2SO_4, and the CV for bulk Pt is outlined in Figure 1-8. The CV curve in Figure 1-8a is that of bulk Pt oxidising LA with each cycle representing a different LA concentration. It was observed that around 1.35V vs a saturated calomel electrode (SCE), anodic current increased with added LA. Peak anodic currents at 1.35V is plotted against LA concentration and is outlined in Figure 1-8b. This graph outlined the dependency of the changing anodic current to LA concentration as current increased in the presence of more LA. The relationship also appeared to be linear in the range of 2-50mM. Similar work conducted by Kim et al. using NiO and $Ni(OH)_2$ powders. CVs for NiO and $Ni(OH)_2$ are observed in Figures 1-9a and 1-9b respectively. The solvent used in this experiment comprised of 0.2M KCl and 0.2M NaOH making it highly basic, but a change in oxidation current was observed in both cases at around 0.5V vs Ag/AgCl when LA concentration was increased. Figures 1-9c and 1-9d show the oxidation currents vs LA concentration for NiO and $Ni(OH)_2$, where a linear correlation is observed between 0-7.76mM, and from 7.76 to 32.76mM of LA in both cases with the higher sensitivity being at the lower concentration range. They also observed that NiO oxidised LA quicker due to the presence of more Ni^{3+} which catalyses the conversion of LA to pyruvic acid in this reaction. Furthermore, their sensitivity studies had also shown that dopamine, ascorbic acid as well as uric acid were not detected by

chronoamperometry (CA) further corroborating the potential specificity of these non-enzymatic materials.

However, as previously stated, the objective is to oxidise LA in isotonic pH conditions in order to create a sensor that is usable in biological applications. Pt is capable of LA oxidation in highly acidic media, while NiO and $Ni(OH)_2$ require alkaline conditions to operate. This thesis will examine how combining Pt with NiO and $Ni(OH)_2$ using the aforementioned Au NP chain self-assembly method to form a catalyst/co-catalyst system that can enhance LA sensing in isotonic pH conditions. And how through the combination of synergistic effects of both elements, and the effect of adjusting these self-assembled NP chain's elemental ratios and morphologies can impact LA sensitivity.

Chapter 2: Nanocomposite Characterization

Synthesizing Ni & Pt nanocomposite chains using AuNP self-assembly

As discussed in Figure 1-6, there are two primary methods used to form the self-assembled chains. The process used throughout this thesis is the method of mixing pre-assembled chains (Figure 1-6a) as this method provided better LA sensing data (discussed in chapter 3) and was easier to reproduce whilst being more stable. To prepare the Pt^{4+} gold nanoparticle (AuNP) chains, 140ul of 4.5mg/mL platinum chloride ($PtCl_4$) solution was added to every mL of citrate capped 10-12nm Au NP solution. The mixture is left on the shaker for around one week until the solution turns dark blue. To prepare the Ni^{2+} chains, 65ul of nickel chloride ($NiCl_2$) was added to every mL of citrate capped 10-12nm Au NP solution but is only left on the shaker overnight as the Ni and AuNPs self-assemble to form chains much quicker than Pt & Au turning the solution into a dark blue color overnight. Observing the NP color change is indicative of agglomeration and chain formation through self-assembly. This is due to the unique properties of AuNP's surface-plasmon resonance (SPR), which has a strong absorption band in the visible light spectrum allowing visual changes to be observed. As the colorimetric behaviour of AuNPs relates to their SPR, changes in their size caused by agglomeration would in turn change the plasmon-resonance frequency, changing the observed color, which can also be observed in greater detail using ultraviolet visual spectroscopy (UV-vis).[28]

The formed Pt cation AuNP chains possess a Pt^{4+} concentration of approximately $1.87x10^{-3}$M, and the produced Ni cation AuNP chains possess a Ni^{2+} concentration of approximately $2.01x10^{-3}$M. The concentrations are similar enough so that the atomic ratios between the two cations can be controlled by their respective solution volumes. The primary AuNP Ni:Pt atomic

ratio studied is a 1:2 Ni:Pt chain structure created by adding two parts Au Pt^{4+} chains to one part Au Ni^{2+}, and the cation self-assembled chains are left on the shaker overnight to mix.

Since the objective is to create an alloy nanocomposite structure containing metallic Pt as well as an oxide of Ni, the pre-assembled cation chains would need to be oxidised and reduced to form $Ni(OH)_2$/NiO and metallic Pt respectively. NaOH is added to the pre-assembled chain structure to increase pH and promote Ni oxidation followed by the addition of small amounts of hydrogen peroxide (H_2O_2). The increase in pH caused by adding NaOH introduces hydroxyl ions which react with Ni^{2+} in solution to form $Ni(OH)_2$, and H_2O_2 acts as another oxidising agent for Ni. After incubating the sample overnight to allow sufficient reaction time, $NaBH_4$ is added to reduce the Pt cations to their metallic state. Fizzing is usually observed at this step, and the solution turns from dark blue to black.

Microscopic Characterization of the Au Nanocomposite Chains

A Field Emission Scanning Electron Microscopy (FESEM or SEM) image of the self-assembled nanocomposite chain structure of the 1:2 Ni:Pt sample is observed in Figure 2-1. The chains can be seen to form a continuous structure of interconnected chains. This creates a porous structure, which should potentially allow for a high surface area for catalysis as more active sites are exposed.[29] This tertiary structure is comporable to that of the Pt and Ru on AuNP chains previously discussed. Furthermore, it was also observed that changing the ratio of Ni to Pt had little influence on the shape of the nanocomposite structure as a 1:10 Ni:Pt AuNP chain strucutre showed the same results (Figure S-1). The differences however between the 1:2 and 1:10 Ni:Pt AuNP composite samples was in their elemental distibution, primarily Ni.

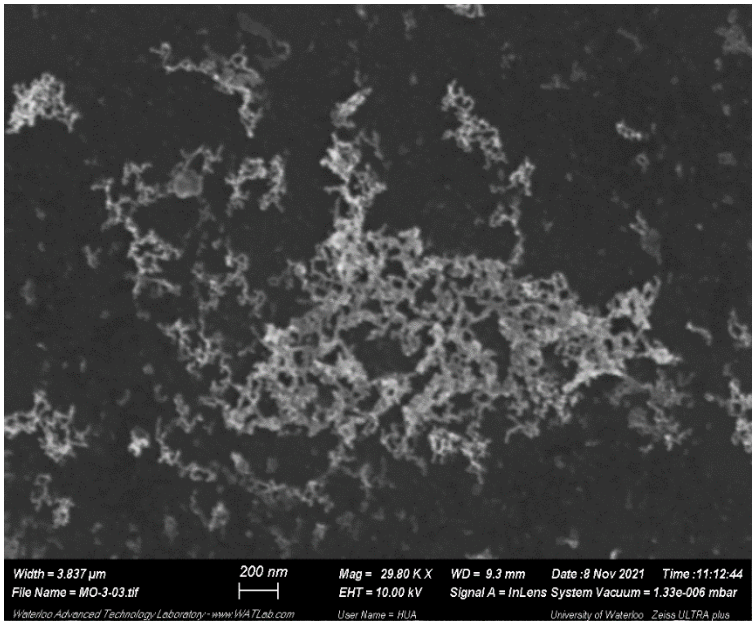

Figure 2-1: SEM image of AuNP pre-assembled nanocomposite chains comprised of 1:2 Ni: Pt.

High Resolution TEM (HRTEM) was used to observe the 1:2 Ni:Pt AuNP chain sample (Figure 2-2a). This method allows the observation of a material's lattice structure, enabling us to distinguish distinct atomic regions.[30] Using X-Ray Diffraction (XRD), it was observed that no peaks were present for Ni AuNPs contrary to observed Pt peaks (Figure S-2), it can be said Ni formed amorphous regions.[31,32] As seen in the 1:2 Ni:Pt AuNP composite chain structure, the AuNP core structure is observed to be roughly 10 - 12nm in diameter, and Pt metal can be observed coating most of the AuNP chain by observing the resolved lattice fringes. The fringes can be seen in Figure 2-2a covering most of the AuNP surface. The areas circled in red are unresolved fringes corresponding to amorphous domains of Ni/NiO/$Ni(OH)_2$. As this sample was prepared using pre-assembled chains, the metals are expected to be distributed in domains, which is primarily the case for Ni. This observation is further confirmed by EELS elemental mapping (Figure 2-2b). The yellow AuNPs are observed as the core structure of the chains, and Pt (green) can be seen forming

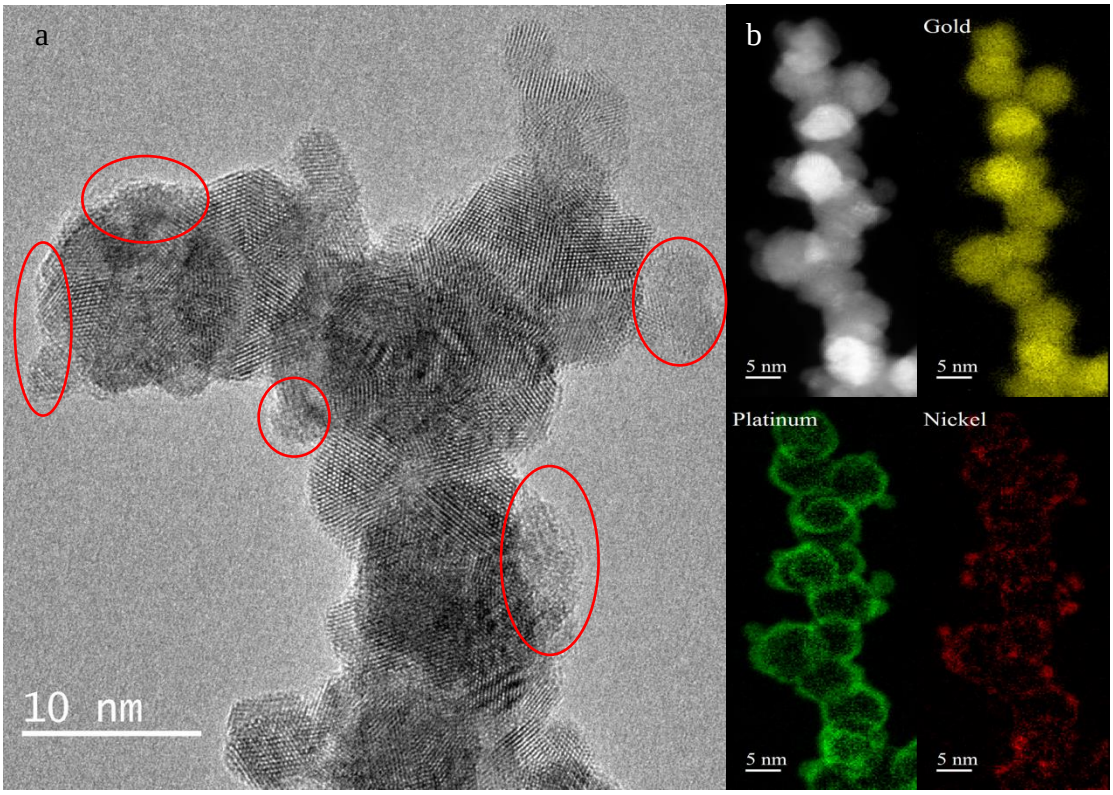

Figure 2-2: HRTEM image of (a) 1:2 Ni:Pt AuNP pre-assembled nanocomposite chains, Ni domains circled in red, and (b) EELS elemental mapping of the chains structure.

a shell around this core structure, with smaller domains of Ni (red) evenly spread throughout the surface of the AuNPs.

Figure 2-3 displays the EELS of 1:10 Ni:Pt AuNP pre-assembled nanocomposite chains. This sample was prepared similarly to the 1:2 Ni:Pt AuNP chains, but with a lower volume of Ni cation AuNP chains during pre-assembly, increasing the atomic ratio of Pt to Ni. While this sample provided visually similar results under SEM and TEM, EELS of Ni (red) shows that there is far smaller and lessser domains of Ni on this sample.

So far, observations indicate towards an interconnected chain-like nanocomposite structure comprising of AuNPs as the core, with a Pt shell covering most of that core accompanied by regions of Ni domains, and that by increasing the amount of Ni cation AuNP chains during the pre-assembly process, we can form chains with more Ni domains after the oxidation and reduction

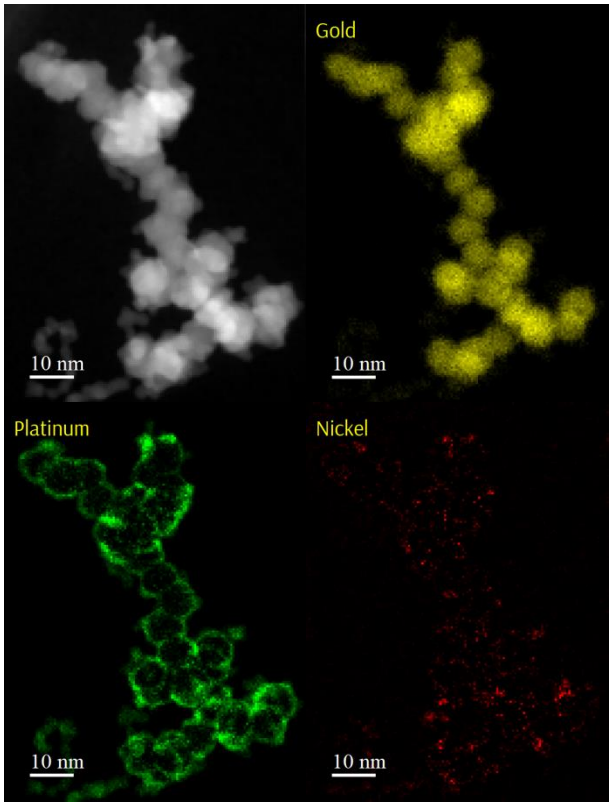

Figure 2-3: EELS elemental mapping of 1:10 Ni:Pt AuNP pre-assembled nanocomposite chains.

steps. However, the objective is to form a catalyst/co-catalyst comprising of metallic Pt and a Ni oxide/hydroxide. And while microscopic techniques allowed the observation of the atomic distribution of these two elements, X-Ray Photoelectron Spectroscopy (XPS) is needed to asses the relative oxidation states of Ni as a Ni oxide is desired.

X-Ray Photoelectron Spectroscopy (XPS) of the AuNP Composite Chains

Ni^{3+} is a desired electrocatalyst for LA oxidation. The Ni and Pt AuNP composite chains were reduced to form metallic Pt, but were also oxidised using NaOH and H_2O_2 to form either NiO, $Ni(OH)_2$, nickel oxyhydroxide (NiOOH), or a combination of these metal oxides. While Ni^{3+} exists as NiOOH, making it the most desireable oxide due to its superior catalytic ability for water oxidation during Oxygen Evolution Reactions (OER) as well as its demonstrated ability to oxidise

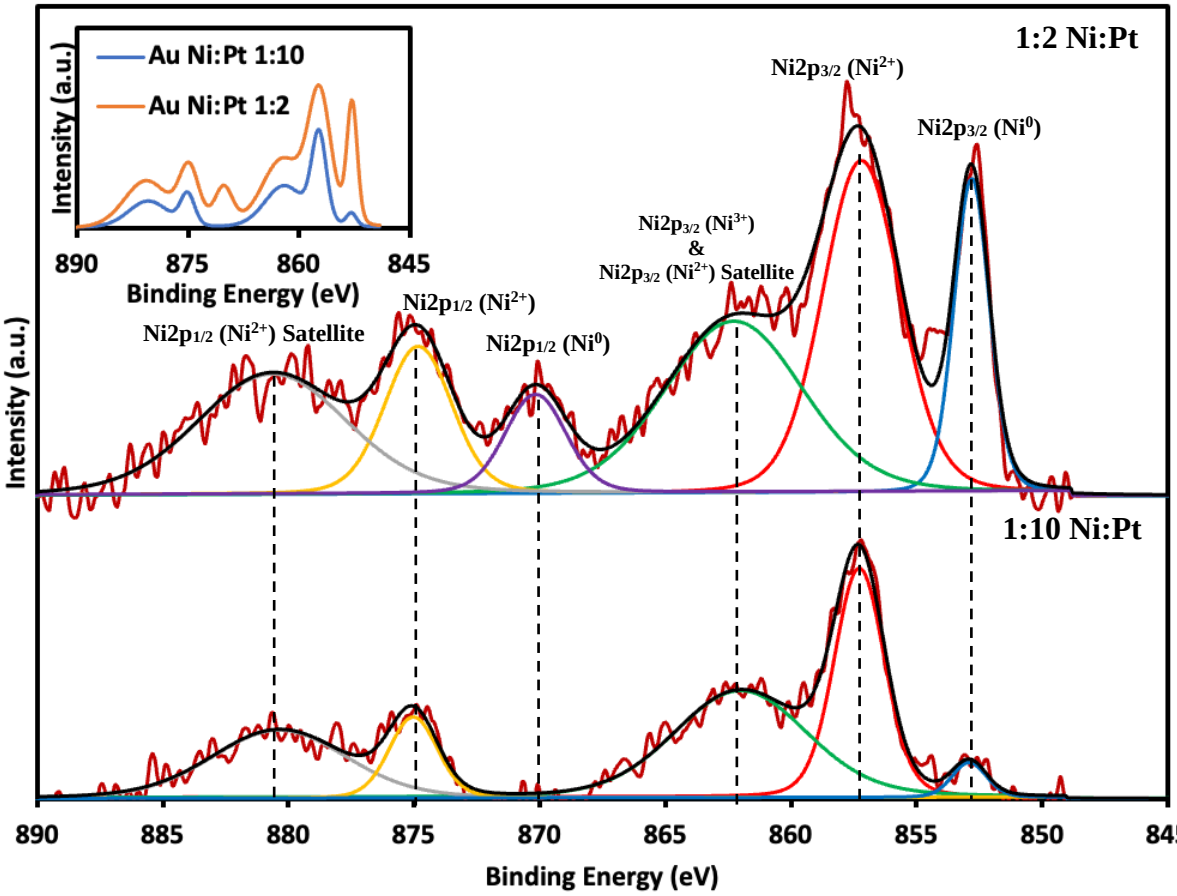

Figure 2-4: High-resolution XPS of the Ni2p spectra for 1:10 & 1:2 Ni:Pt AuNP pre-assembled nanocomposite chains.

LA into pyruvic acid and free electrons in alkaline conditions, it is also one of the least stable forms of Ni oxides.[33]

XPS of the Ni spectrum was conducted on the 1:2 and 1:10 Ni:Pt AuNP pre-assembled chains that have been oxisied using NaOH and H_2O_2, followed by reduction using $NaBH_4$. The backgrounds were subtracted, the peaks fitted, and signal denoised using CasaXPS, and the results can be seen in Figure 2-4. The 1:2 Ni:Pt contained higher amounts of Ni, which was apparent in EELS, and is also observed in figure 2-4 (inset) showcasing that the relative intensity of the 1:2 sample was higher than the 1:10. Both the $Ni2p_{3/2}$ and $Ni2p_{1/2}$ peaks were observed at 857.3eV and 875.1eV respectively in both the 1:2 and 1:10 Ni:Pt samples. These characteristic peaks

indicate the presence of a Ni^{2+} oxide in both samples, and although it is possible to fit multiple peaks to help determine the distribution between NiO and $Ni(OH)_2$, the spectrum resolution was not high enough to accurately fit those peaks as there are several methods of peak fitting and analysis is usually subjective.[34] The presence of Ni^{3+} is also not easy to quantify as it doesn't show a distinct peak. However, NiOOH has a major Ni^{3+} $Ni2p_{3/2}$ peak at 861.0eV, which overlaps with the Ni^{2+} $Ni2p_{3/2}$ satellite peak.[35] The relative presence of Ni^{3+} between the different nanocomposite samples can hence be estimated by comparing the relative intensities of both the Ni^{2+} $Ni2p_{3/2}$ to its satellite peak as the presence of Ni^{3+} would contribute to that satellite peak if present. This method will not necessarily prove the presence or existence of Ni^{3+} in any of the tested samples, but is instead used here to estimate the relative changes in compositions of the different Ni states to help estimate which sample would have the greatest amount of Ni^{3+} relative to Ni^{2+}. In the 1:2 Ni:Pt sample, the intensity ratio of the $Ni2p_{3/2}$ Ni^{3+}:Ni^{2+} was found to be 0.522, while for 1:10 Ni:Pt that was at 0.468. The relative intensities are similar and can be considered within margin of error given the signal noise and optimal peak fitting, but the Ni^{3+} composition in the 1:2 sample appears to be higher indicating the sample might contain relatively more NiOOH.

Where these samples greatly differ however was in the formation of metallic Ni. The Ni^0 $Ni2p_{3/2}$ was observed on both samples at 852.6eV, but with a much greater intensity in the 1:2 Ni:Pt sample. Metallic Ni's $Ni2p_{1/2}$ peak was also observed at 870eV in the 1:2 sample, but was not significant enough to be detected in the 1:10 sample, meaning that more metallic Ni was formed in the 1:2 sample. This may have been facilitated by the $NaBH_4$ reduction step intented to produce metallic Pt, however Au Ni nanocomposite chains that have been reduced without the presence of Pt did not show any metallic Ni peaks (Figure 2-5), implying their instability, which can also be visually observed as reduced Au Ni samples changed colors from black to purple

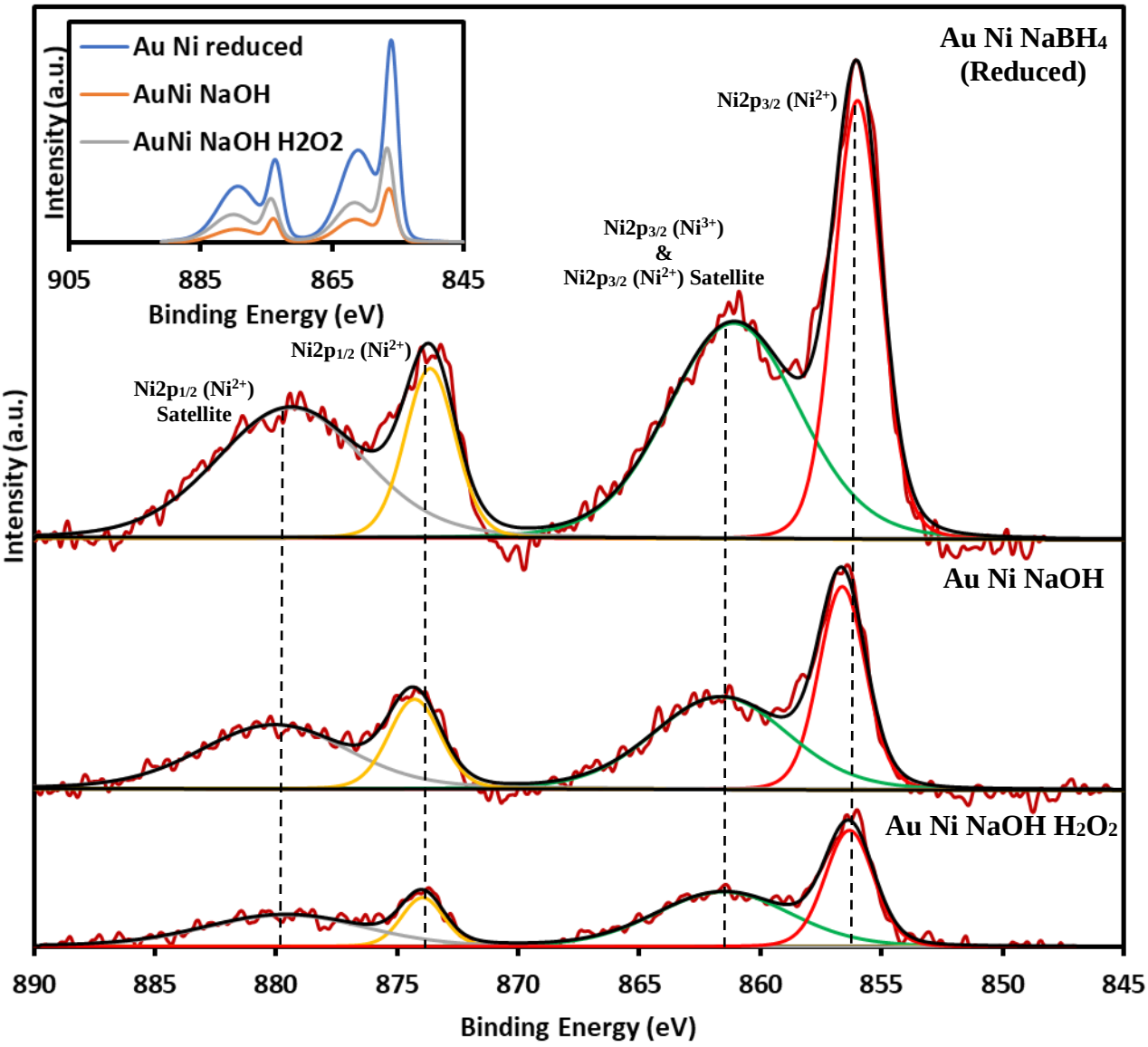

Figure 2-5: High-resolution XPS of the Ni2p spectra for Au Ni reduced, Au Ni with NaOH only and Au Ni with NaOH and H_2O_2 pre-assembled nanocomposite chains.

indicating the breakage of the nanocomposite chains as this color is correlated to a smaller nanoparticle size.[36] This may suggest that the presence of Pt metal aids in the stability of metallic Ni during the reduction step forming an alloy in the process.

To further test the effectiveness of Ni oxidation, three Ni AuNP nanocomposite chain samples were prepared. The first sample was the Ni cation chains reduced using $NaBH_4$, the second was oxidised using NaOH only, and the third was oxidised using both NaOH as well as H_2O_2. The

Ni2p XPS spectra is observed in Figure 2-5. As previously mentioned, the metallic Ni peak was not observed on the reduced Ni sample owing to its instability. However, both $Ni2p_{3/2}$, $Ni2p_{1/2}$ as well as their satellite peaks were observed on all three samples indicating the presence of a Ni oxide. To determine the relative NiOOH composition, the $Ni2p_{3/2}$ Ni^{3+}:Ni^{2+} peak intensity ratio was used and the calculated values were 0.494, 0.472 and 0.456 for reduced Au Ni, Au Ni with NaOH and Au Ni with NaOH and H_2O_2 respectively. This may suggest that Ni oxidation using

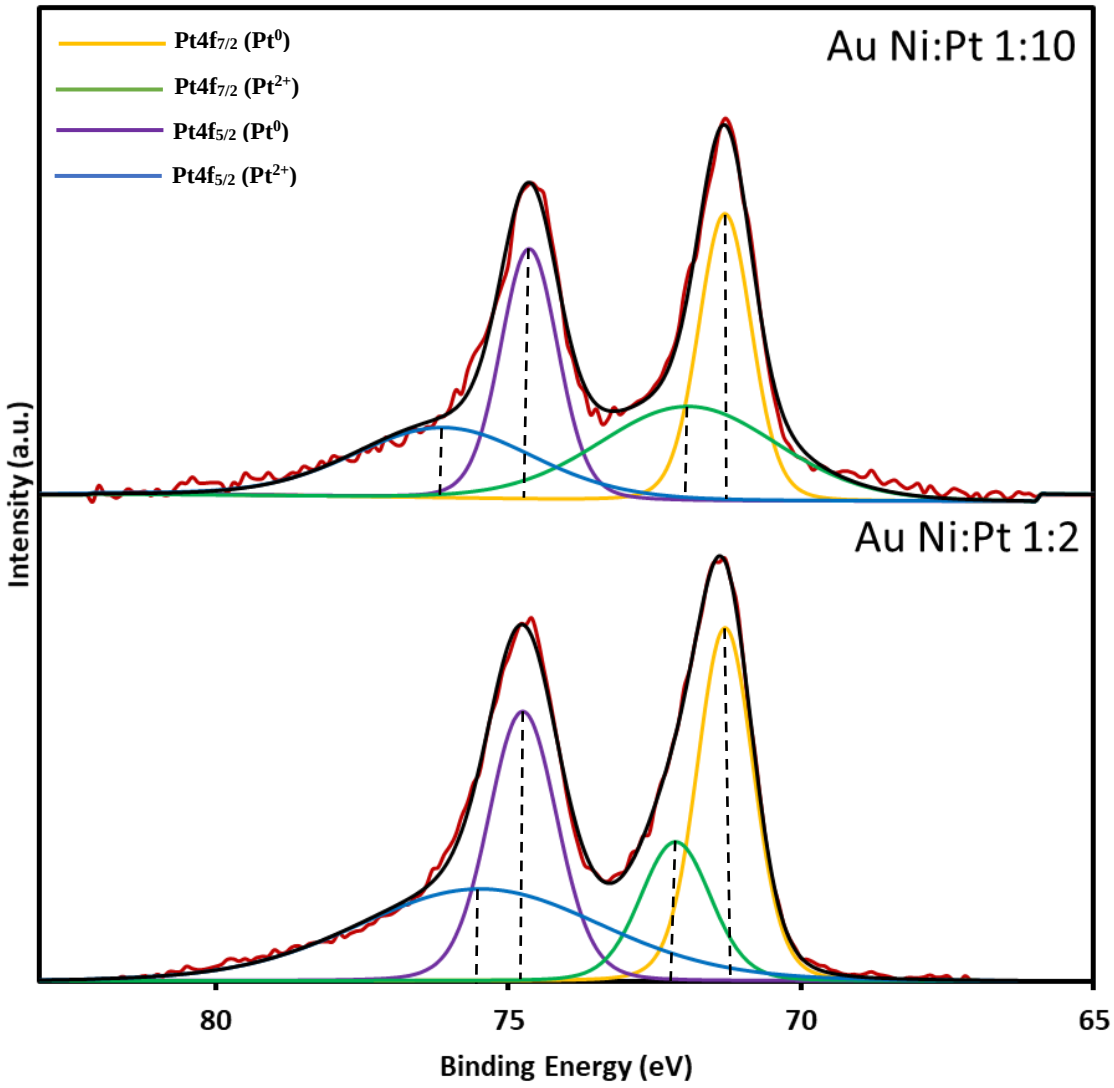

Figure 2-6: High-resolution XPS of the Pt4f spectra for 1:10 & 1:2 Ni:Pt AuNP pre-assembled nanocomposite chains.

NaOH and H_2O_2 may not be the most suitable method to produce relatively more Ni^{3+} states if present, however combining Ni with Pt did show an increase in the relative Ni^{3+} composition as is demonstrated in the 1:2 Ni:Pt sample.

As for the formation of metallic Pt by $NaBH_4$ reduction, both the 1:2 and 1:10 Ni:Pt Au nanocomposite chains were mostly comprised of metallic Pt, with some Pt^{2+} either in the form of platinum oxide (PtO) or platinum hydroxide ($Pt(OH)_2$). XPS spectra for Pt4f can be seen in Figure 2-6. The $Pt4f_{7/2}$ peak for metallic Pt was the dominant peak with a binding energy of 71.3eV in both samples. The fitted peaks also indicated that there was some Pt that was not fully reduced (72.2eV), possibly existing as PtO or $Pt(OH)_2$, but no Pt^{4+} states remained in the sample which would theoretically have a $Pt4f_{7/2}$ peak at around 74.4eV which is not observed.[37] As the valence band spectrum splitting for Pt4f from $Pt4f_{7/2}$ to $Pt4f_{5/2}$ is 3.3eV, the second peak observed at 74.7eV and 75.5 corresponed to the Pt^0 and Pt^{2+} $Pt4f_{5/2}$ peaks respectively. This confirms that most Pt on

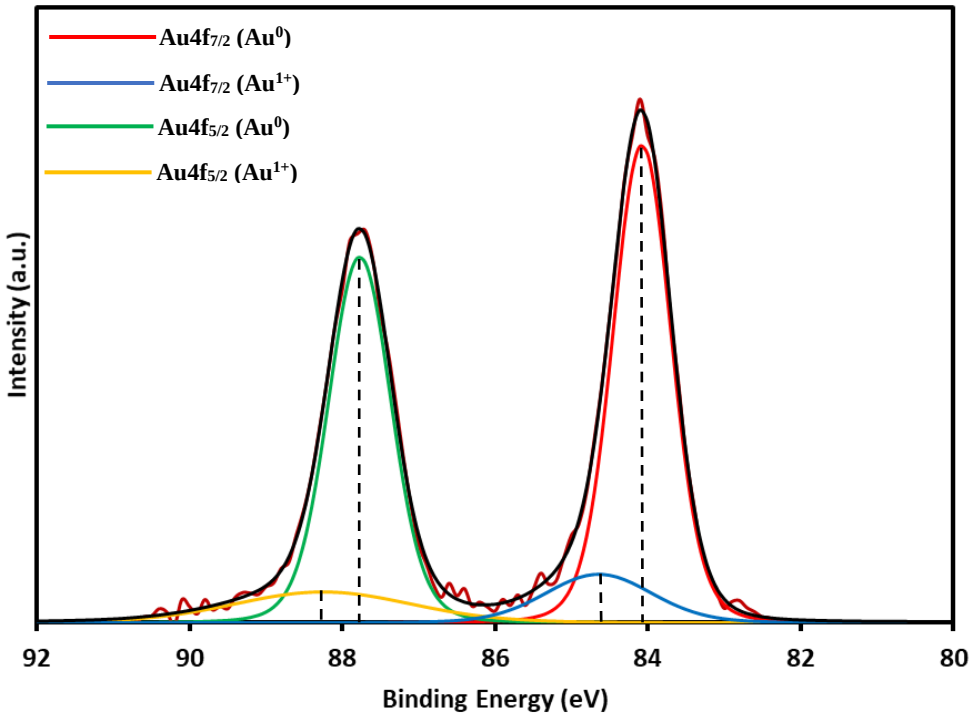

Figure 2-7: High-resolution XPS of the Au4f spectra for 1:2 Ni:Pt AuNP pre-assembled nanocomposite chains.

the nanocomposite chains has been successfully reduced to their metallic states, forming a shell around the AuNPs as confirmed by HRTEM and EELS.

As for the AuNP core, Au remained unaffected by the oxidation or reduction reactions as all tested samples showed a similar Au4f XPS spectrum. A sample spectrum is shown for the 1:2 Ni:Pt AuNP nanocomposite chains in Figure 2-7. Metallic gold peaks were observed at 84.1eV and 87.7eV for $Au4f_{7/2}$ and $Au4f_{5/2}$ respectively, aligning with literature on metallic AuNPs.[38] The very small Au^{1+} peaks observed are normal and are usually found in citrate reduced AuNPs.

Overall, combinng SEM, HRTEM, EELS and XPS data, we can infer that the prepared Ni:Pt AuNP pre-assembled nanocomposite chain samples that have been treated with NaOH, H_2O_2, and $NaBH_4$ respectively form a porous inter-linked chain structure comprised of a Au core with a metallic Pt shell, and smaller domains of oxidised Ni distributed around the Pt shell. This thesis will demonstrate that this metal and metal oxide combination enhances LA detection in isotonic pH as will be discussed in Chapter 3.

Chapter 3: Nanocomposites Lactate Sensing

Validating LA Oxidation Capability Using Pt & Ni AuNP Nanocomposite Chains

Literature has demonstrated that Pt metal as well as Ni oxide/hydroxide can oxidise LA under acidic and basic conditions respectively. In order to validate the AuNP nanocomposite chain's catalytic ability for LA oxidation relative to bulk electrodes, separately prepared $NaBH_4$ reduced Pt AuNP chains as well as NaOH and H_2O_2 treated Ni AuNP chains were used to corroborate the LA oxidation capability. To confirm the catalytic ability of Pt metal, the reduced Pt AuNP chains were drop cast on a glassy carbon electrode (GCE), and CV cycled vs a Ag/AgCl

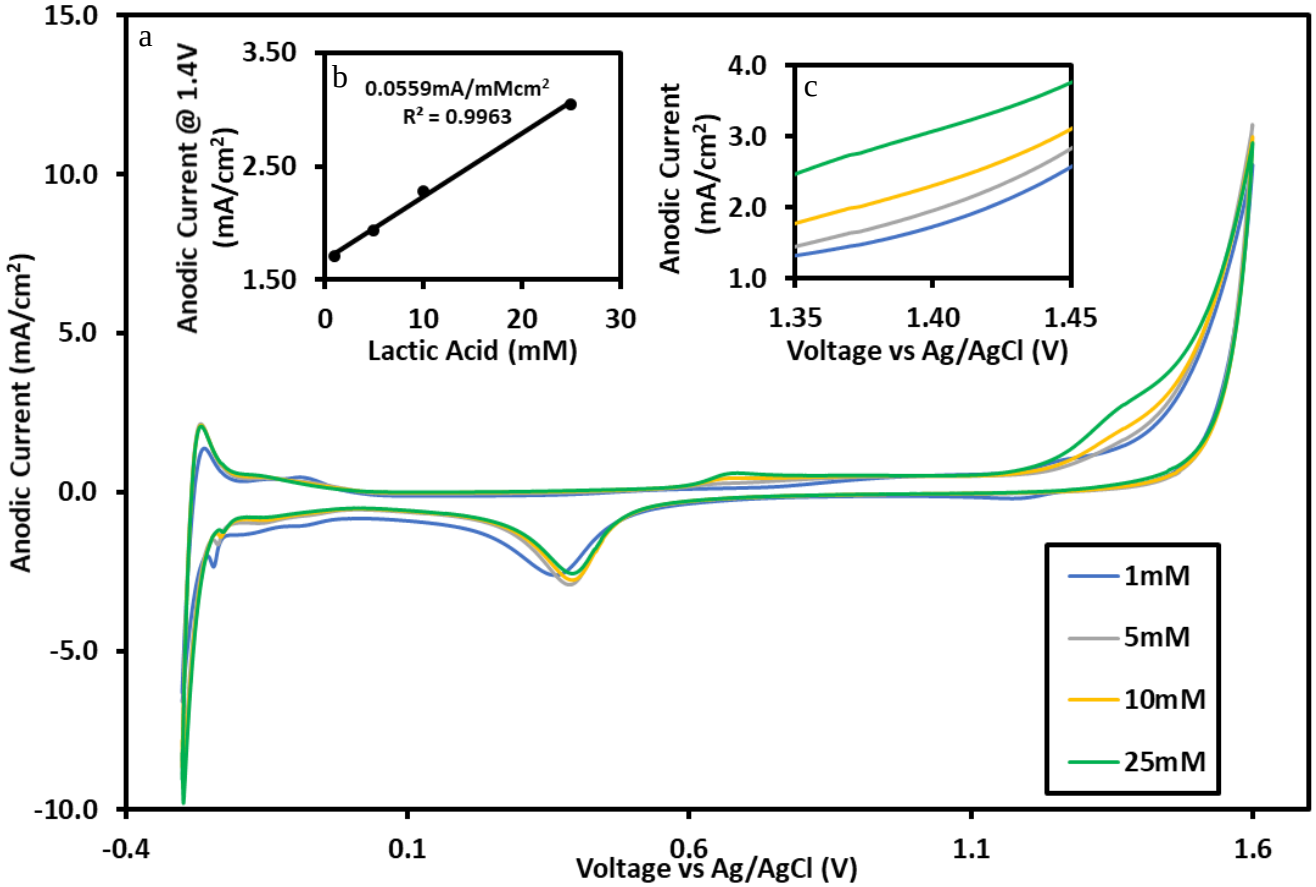

Figure 3-1: CV curve of Pt AuNP self-assembled chains in different LA concentrations in 0.5M H_2SO_4 (a). The plotted anodic currents vs lactate concentrations at an oxidation potential of 1.4V (b), and CV cycle close-up (c).

reference electrode in a 0.5M H_2SO_4 solution containing different LA concentrations, and the results are shown in Figure 3-1.

The CV was run from 0.3-1.6V for three cycles each in 1, 5, 10 and 25mM LA , and cycle 2 was plotted (Figure 3-1a). An oxidation peak can be spotted around 1.2-1.5V and a close-up of this is seen as an inset in Figure 3-1c. The currents were plotted at 1.4V vs their respective LA concentrations (Figure 3-1b) and a linear response was observed. These results were comparable to that of literature seen (Figure 1-8) showing that the Pt in AuNP chains have the potential to functionalize as catalysts as well as their bulk material counterparts.

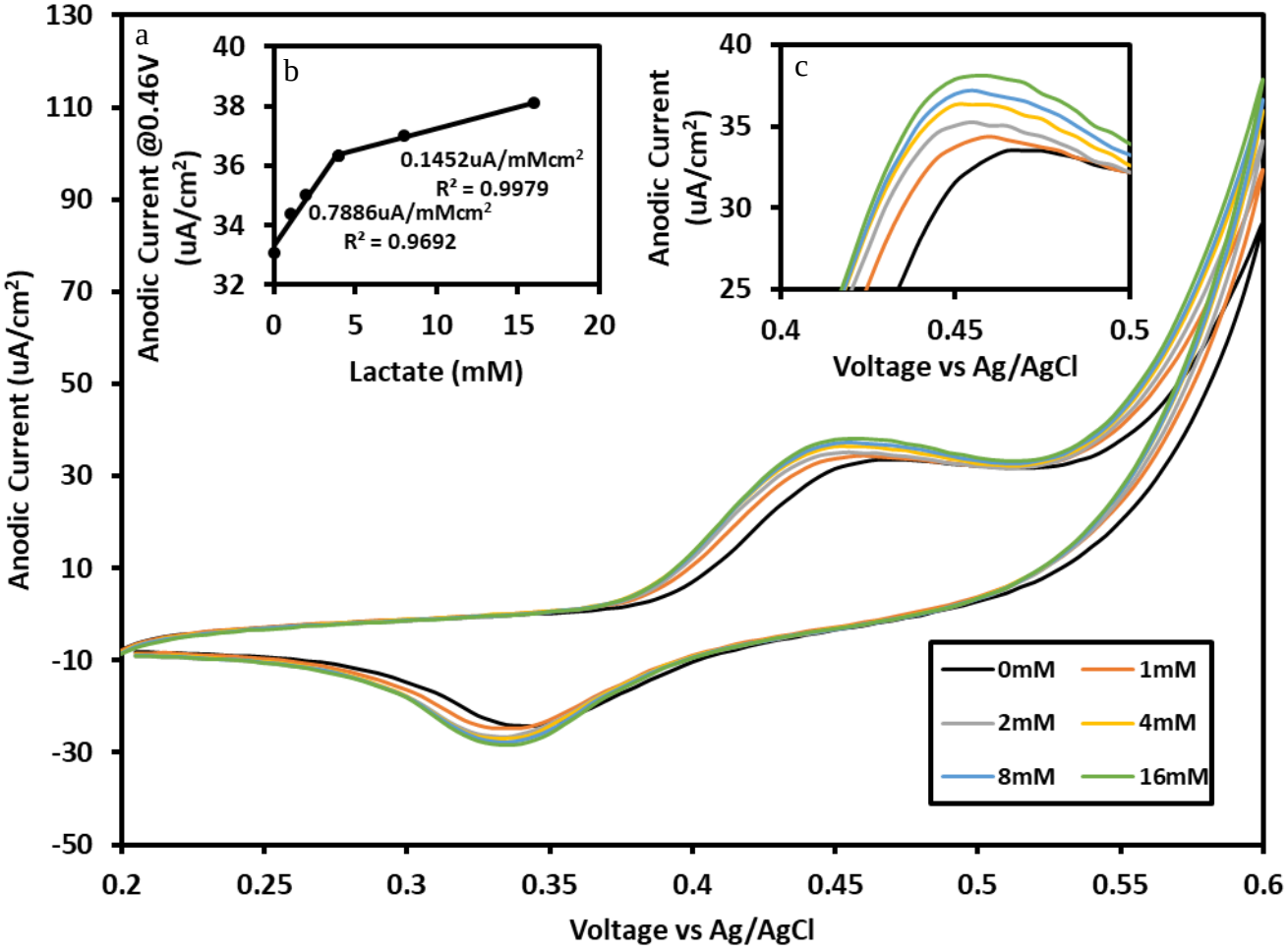

Figure 3-2: CV curve of Ni AuNP self-assembled chains in different LA concentrations in 0.2M NaOH and 0.2M KCl (a). The plotted anodic currents vs lactate concentrations at an oxidation potential of 0.46V (b), and CV cycle close-up (c).

The same experiment was done using Ni AuNP chains treated with NaOH and H_2O_2 in 0.2M KCl and 0.2M NaOH to provide basic conditions, and results are seen in Figure 3-2. Similar to literature, LA oxidation occurred at around 0.46V. When looking at the CV cycle shape (Figure3-2a), it was closest to that of NiO (Figure 1-9a). The current values were plotted vs their respective LA concentrations at 0.46V and the data is presented in Figure 3-2b. Two linear regions can be observed, from 0-4mM, and from 4-16mM. Although sensitivity was lower than that of bulk Ni electrodes, trends remained very similar. This is an indication that Ni AuNP chains are capable of oxidising LA in basic conditions, and that overall, the metal and metal oxide nanocomposite chains have the ability to function as catalysts similar to their bulk material counterparts.

Testing Pt & Ni AuNP Nanocomposite Chains in Isotonic pH Conditions

To assess the LA oxidation capability of the nanocomposite chains in neutral or isotonic pH conditions, phosphate buffered saline (PBS) was used as a solvent. PBS is a buffer that possesses a pH of around 7.4 and is used to simulate many biological applications.[39] 2X PBS was used in order to increase buffering capacity to prevent large changes in pH from the addition of LA. $NaBH_4$ treated Pt AuNP chains as well as NaOH and H_2O_2 treated Ni AuNP chains were drop cast on a GCE and coated with a layer of Nafion. They were conditioned for 200 cycles in 2X PBS using a Pt counter electrode and a SCE reference. A continuous current of 1.44V was ran using chronoamperometry (CA). LA was added at different time intervals increasing its concentration, and the data for Ni AuNPs is plotted in figure 3-3. Looking at the graph, it was hard to distinguish an oxidation event caused by a change in current when increasing LA concentration. The dotted lines show when LA was added to the system, and a real-time response was not properly observed. This was also the case when observing CA for Pt AuNPs. This indicates that the potential for Pt

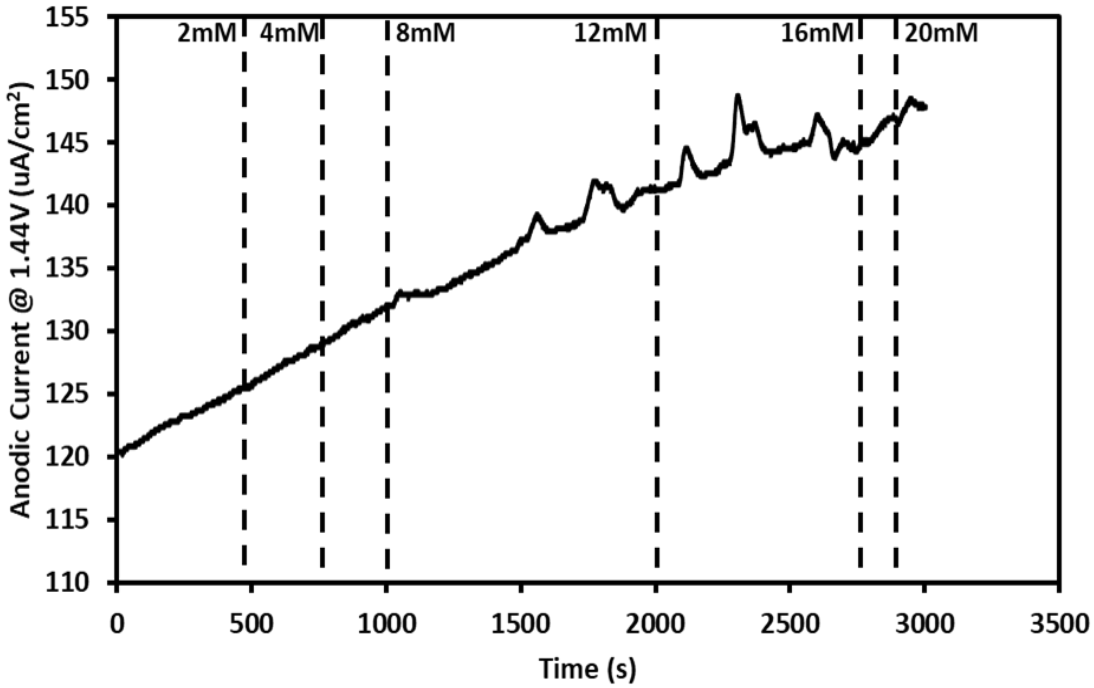

Figure 3-3: Real-time LA detection using CA at an oxidation potential of 1.44V vs SCE for Ni AuNP nanocomposite chains in a 2X PBS solution. Each vertical line shows LA addition.

or Ni AuNPs for real-time LA detection is not ideal, at least when operating individually. However, this changes when looking at combined Ni and Pt nanocomposite chains.

Ni Pt Pre-assembled Nanocomposite Chain LA Sensitivity

As XPS data showed, combining Ni and Pt chains forms a porous inter-linked chain structure comprised of a Au core with a metallic Pt shell, and smaller domains of oxidised and metallic Ni distributed around the Pt shell. The hypothesis is that by combining a catalyst and co-catalyst, the catalytic alloy can bring about synergestic effects and improve LA detection. To test this theory, the oxidised and reduced 1:2 and 1:10 Ni Pt Au pre-assembled nanocomposite chains were tested for LA sensitivity in 2X PBS. Samples were drop cast on a GCE and coated with a layer of Nafion. They were conditioned for 200 cycles in 2X PBS using a Pt counter electrode and a SCE reference. LA was added and three CV cycles were run in each concentration, and the anodic currents for the second CV cycle were used to assess sensitivity and linearity. Figure 3-4 shows

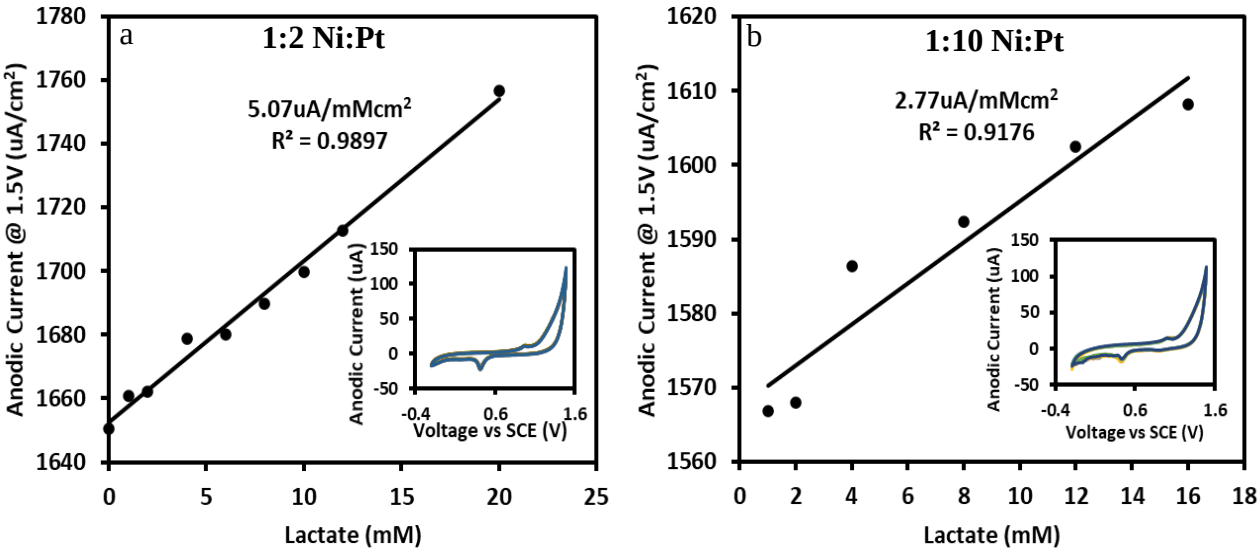

Figure 3-4: The plotted anodic currents vs lactate concentrations at an oxidation potential of 1.5V vs SCE for 1:2 Ni:Pt (a) and 1:10 Ni:Pt (b) oxidised and reduced pre-assembled AuNP nanocomposite chains in a 2X PBS solution. Insets are their respective second CV cycles in all plotted lactate concentrations.

the anodic currents at 1.5V vs LA concentration. Currents at 1.5V were used as they had the best sensitivity and linearity in both samples. It was observed that both samples showed a linear increase in current with increasing LA concentration, with the 1:2 Ni:Pt (Figure 3-4a) chains having a higher sensitivity than the 1:10 Ni:Pt (Figure 3-4b) sample being 5.07 and 2.77uA/mMcm^2 respectively. CV data was also similar (Figure 3-4 insets) with the greatest change in current being observed at 1.5V for both samples, which was hard to observe without plotting the data. There is a small oxidative peak observed for both samples around 1V (Figure 3-4 inset) which could likely be caused by Pt oxidation since it was not found in samples that did not contain Pt.[40,41] The sample containing more Ni composition and possibly less Pt was more sensitive to LA. The Pt containing samples were also less sensitive in neutral conditions because acidic conditions needed to drive the oxidation reaction for Pt are not there, as one explanation could be that while LA retains its proton in highly acidic conditions, it more easily deprotonates in PBS as it has a pK_a of 3.85 at 25°C, which is much lower than the pH of PBS buffer of 7.4, which may have an impact

on the reaction dynamics as will be later discussed.[42] As for Ni, it is likely that to oxidise LA, a higher potential was probably required to convert Ni^0/Ni^{2+} to Ni^{3+} in non basic conditions.

The limit of detection for LA was also calculated for the 1:2 Ni:Pt sample. This is the lowest amount of LA that can be detected with a certain degree of certainty, or high statistical significance.[43] Sensors are usually less reliable when measuring concentrations closer to 0, and although they can detect the presence of a certain analyte lower than the limit of detection, there is a degree of uncertainty. The detection limit is hence the lowest concentration of analyte that can be significantly distinguished from 0mM, although this still does not necessarily mean that it could be quantified at that limit.[44] There are several methods of statistically calculating the limit of detection, in this case, the calibration graph, or LA response (from Fig 3-4a) was used to calculate the limit of detection using the following equation:

$$\text{Limit of Detection} = 3.3\sigma / S \qquad (3\text{-}1)$$

Where σ is the standard deviation of the response's intercept at 0 for the fitted sensitivity curve, and S is the slope of that fitted sensitivity curve line.[45] The limit of detection of lactate using the 1:2 Ni:Pt was calculated to be 3.52mM. This means that it can be said with high statistical significance that LA is being detected at concentrations higher than 3.52mM rather than detecting fluctuations or changes in background noise for instance that can provide a false positive.[44] Although the sensor has demonstrated ability to detect LA at lower concentrations, it cannot be said that LA was detected with high statistical significance until the limit of detection is reached. The limit of detection can be further improved with sensor optimization; however, this is still acceptable as ischemic events that cause ALs also cause LA levels to exceed 9mM, which is much higher than the current limit of detection.

Where the combined chains however sets itself apart from individually prepared Pt or Ni oxides is in continuous LA monitoring. The 1:2 Ni:Pt AuNP pre-assembled chains were superior in terms of real-time detection using CA. Using 2X PBS as a buffer, the 1:2 Ni:Pt sample was conditioned for 200 cycles from -0.2-1.5V, then CA was ran at 1.44V vs a SCE which was found to be the optimal potential for continuous LA sensing. The solution was stirred at 200rmp, and LA was added in small increments and current changes were monitored. The overall CA data is presented in Figure 3-5. The concentrations labelled on the figure represent the total amount of LA in the system. After current was left to stabilize, LA was added and a current increase was observed. The following addition of LA was made after the increased current became more stable, until a total of 18mM was introduced to the system. The overall graph shows an upwards trend

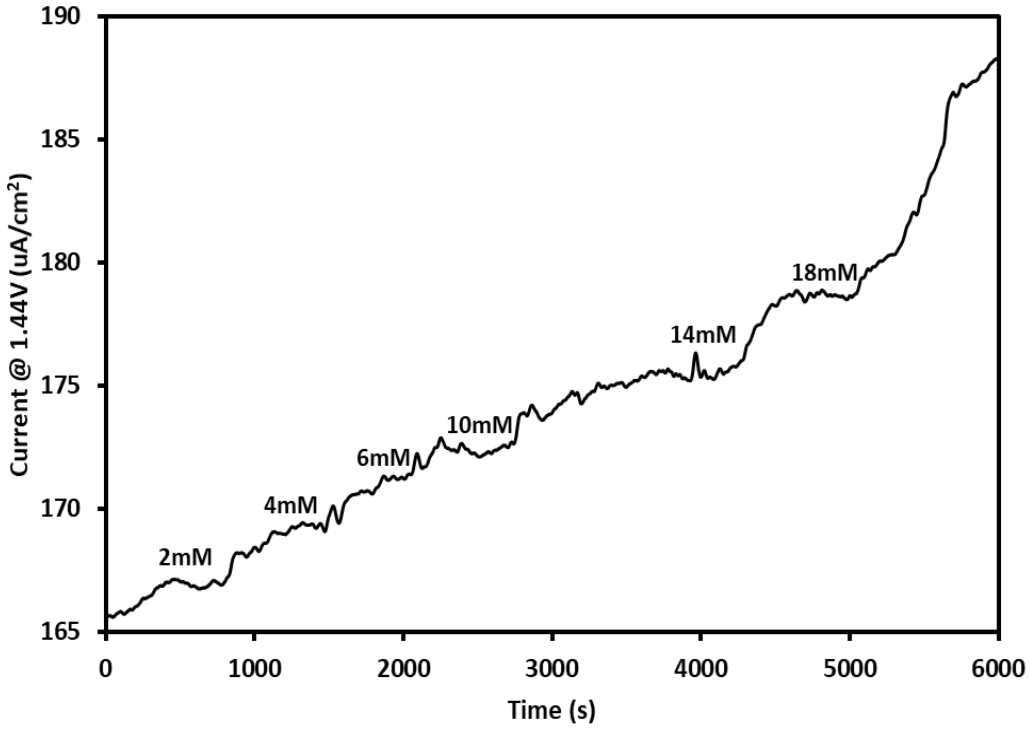

Figure 3-5: Real-time LA detection using CA at an oxidation potential of 1.44V vs SCE for 1:2 Ni:Pt oxidised and reduced pre-assembled AuNP nanocomposite chains in a 2X PBS solution.

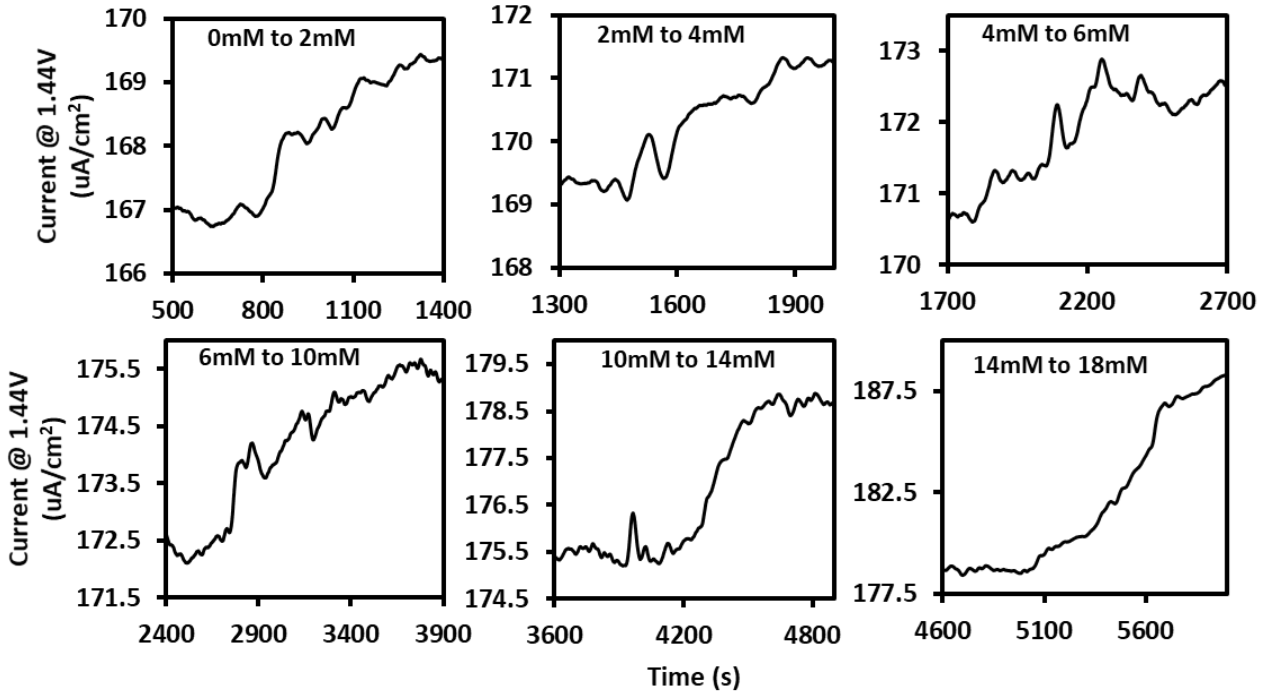

Figure 3-6: A close-up look at the real-time LA detection using CA at an oxidation potential of 1.44V vs SCE for 1:2 Ni:Pt oxidised and reduced pre-assembled AuNP nanocomposite chains in a 2X PBS solution. Each graph represents an event when LA was added to the system.

with larger changes in current when LA was added. There are also some periods of relative stability indicating the system has reached equilibrium before adding additional LA.

To present a more detailed analysis, a breakdown of the individual LA additions is presented in Figure 3-6. Here, changes can be observed in more detail. When going from 0 to 2mM LA, the current increased by about 2.5uA/cm^2, which is equivalent to 1.25uA/mMcm^2. While sensitivity is lower than that observed using CV, it is because the best linearity for CV runs was at 1.5V as opposed to 1.44V which gave the best results using CA. Sensitivity remained rather steady at about 1uA/mMcm^2 between additions, with the exception of the last LA addition.

Overall, results imply that LA can be detected using the Ni:Pt nanocomposite chains and that by combining both elements, there was a much greater ability to continuously monitor LA in isotonic pH conditions, which may be due to synergestic effects. However, there still remains a lot

of room for improvements in terms of sensitivity and sensor response time, which will be touched upon in chapter 4.

Testing LA Specificity and Hysteresis

A major advantage of enzymatic LA sensors is its specificity. Although catalytic non-enzymatic sensors may not be as specific, there are certain methods used to increase specificity towards a certain analyte, such as using certain potentials for detection, and adding additional coatings that can prevent interferances from other analytes. The first step was to test whether other analytes can interfere with our LA detection by testing sensitivity to other analytes. In order to test this, sensitivity to the similarly structured acetic acid, which is also a weak acid that contains a corboxyl group, in addition to glucose, a common biological analyte as well as a common research target for non-enzymatic catalysis, were used.

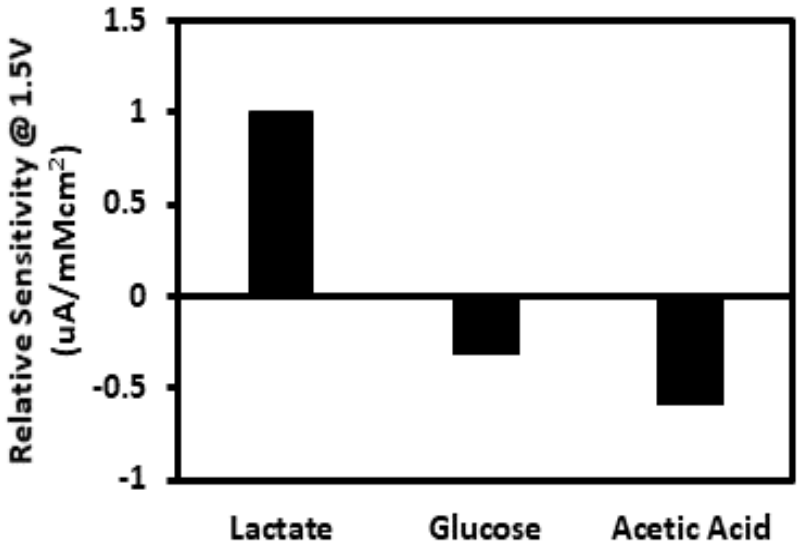

Figure 3-7: The plotted relative sensitivities of lactate, glucose and acetic acid at an oxidation potential of 1.5V vs SCE for 1:10 Ni:Pt oxidised and reduced pre-assembled AuNP nanocomposite chains in a 2X PBS buffer.

Selectivity data is presented in Figure 3-7. Similar to the method used to detect LA, using the 1:10 Ni:Pt oxidised and reduced pre-assembled AuNP nanocomposite chains, the sample was drop cast on three separate GCEs and coated with Nafion. They were then conditioned for 150 cycles from -0.2-1.5V vs SCE and each analyte was added to their respective electrode and three CV cycles ran from -0.2-1.5V vs SCE while using the results for the second cycle. The bar graph represents the relative sensitivities calculated between analytes when measuring sensitivity using anodic currents at 1.5V. Not only did LA response have the highest sensitivity, but it also had the only positive correlation. The lower sensitivities towards other analytes relative to that of LA, imply decent selectivity towards LA, although not perfect. This also implies that the increases in currents are likely due to the increases in LA concentration.

Hysteresis testing further proves this, while also investigating another important sensor parameter. Hysteresis can have several definitions depending on the certain application and sensor type it is being referenced to.[46] In this case, it is how close the sensor's output is at a certain concentration regardless of whether the change was in a positive or negative direction to get to that concentration. To test this, LA was added in increments to the stirred 2X PBS solution, and three CV cycles were run from -0.2-1.5V vs SCE. The solution was then diluted to the desired LA concentration using 2X PBS buffer while keeping the total volume identical, and measurements taken. Results for this is presented in Figure 3-8. The data points plotted represent anodic current at 1.5V vs SCE. It can be seen that for the 1:2 Ni:Pt AuNP pre-assembled nanocomposite chains, current increased with increasing LA concentration, and decreased with decreasing concentration.

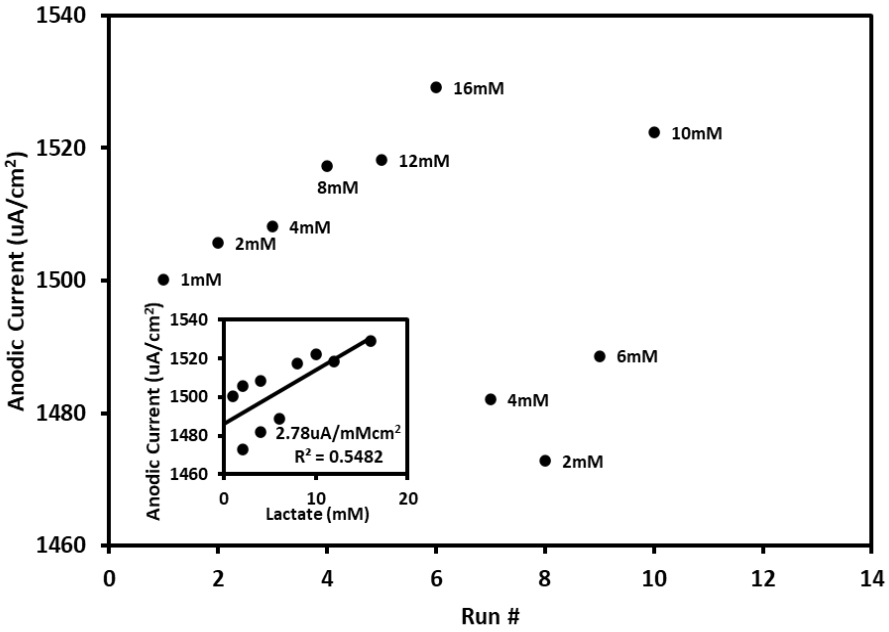

Figure 3-8: The plotted hysteresis for lactate at an oxidation potential of 1.5V vs SCE for 1:2 Ni:Pt oxidised and reduced pre-assembled AuNP nanocomposite chains in a 2X PBS solvent.

The graph showed that the current is dependent on the changes in LA concentration. Hysteresis can be quantified by observing the linearity of the sensitivity curves when plotting LA concentration vs current (Figure 3-8 inset). Although it is observed that current significantly dropped with LA concentration in the 1:2 Ni:Pt sample, it is likely because the sample did not have enough time to settle to take a proper measurement. CA was run at 1.44V vs SCE on 1:2 Ni:Pt, this time starting with 18mM LA and diluting the 2XPBS buffer while stirring (Figure 3-9). It was observed that as the solution was diluted to decrease LA, current decreased, and the decrease in current corresponded with the amount of dilution incurred on the buffer to remove LA. What is also observed is that current also slowly increases over time after each dilution. When left for a long period, it eventually reaches equilibrium at a current similar to the one measured when increasing LA, but this also means that the sample had a long settling time. In this case hysteresis may have been overestimated, and a better testing methodology is probably needed to produce

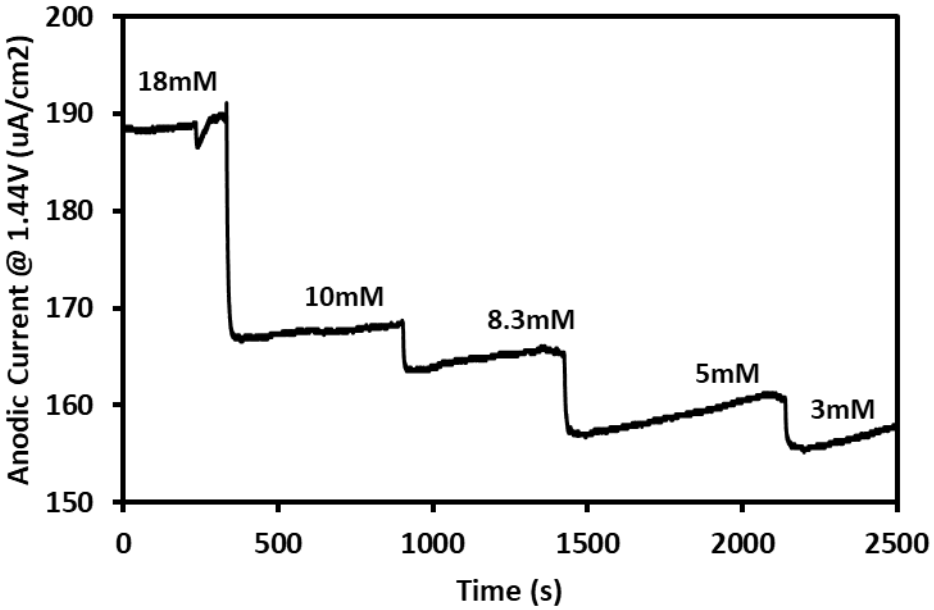

Figure 3-9: Real-time LA detection with decreasing LA concentration using CA at an oxidation potential of 1.44V vs SCE for 1:2 Ni:Pt oxidised and reduced pre-assembled AuNP nanocomposite chains in a 2X PBS solution.

more accurate data. Overall, the data however still indicates that changes in current are correlated to LA concentration.

LA Detection Conclusion

Combined Ni:Pt pre-assembled chains showed good linearity with increasing LA concentration in neutral pH, indicating the potential for a combination to be used as future non-catalytic LA sensors. While oxidised Ni AuNPs and Pt AuNPs at neutral pH did not show good real-time LA detection, best continuous LA detection results were obtained by combining both elements. Through the combination of Ni and Pt AuNPs, most notably in a 1:2 Ni:Pt ratio by pre-assembling N^{2+} and Pt^{4+} AuNP chains, then oxidising using NaOH and H_2O_2, and reducing with $NABH_4$, the produced nanocomposite had a good response for continuous LA monitoring and achieved good linearity while managing decent sensitivity and hysteresis. This sample most notably allowed for the continuous real-time detection of changes in LA concentration in neutral

pH, taking one step closer towards the primary objective of making a stable non-enzymatic sensor to detect ischemia and ALs.

Proposed Reaction Mechanism

Theoretically, to detect LA using Ni oxides in basic conditions, $Ni^{0/2+}$ is first oxidised to Ni^{3+} if none is already present on the catalyst surface in the form of NOOH. This is more easily achieved in basic conditions since readily available OH^- groups can adsorb onto $Ni(OH)_2$ at potentials higher than 0.3V in basic conditions converting it to NiOOH.[47] This is demonstrated by the following eq:

$$Ni(OH)_2 + OH^- \longrightarrow NiOOH + H_2O + e^- \qquad (3\text{-}2)$$

Since this oxidation reaction can theoretically take place with more ease in basic conditions, it could be the case that a higher potential is required in more neutral conditions to drive this reaction to take place on the Ni oxide catalyst surface. Ni^{3+} is also desirable as it is a well-established electrocatalyst capable of oxidising many organic compounds. Once Ni^{3+} species have been established on the catalyst surface, LA oxidation to pyruvic acid takes place reducing the NiOOH in the process following this reaction:

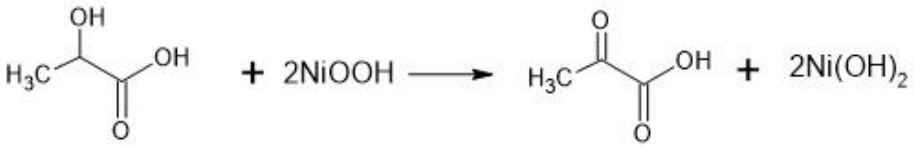

(3-3)

This could theoretically mean that samples with more Ni^{3+} could oxidise LA quicker and at possibly lower potentials if reaction 3-2 is the limiting step, therefore it could be better to aim to fabricate future iterations of Ni AuNP nanocomposites with a higher Ni^{3+} composition.

How Pt metal oxidises LA however is a more complicated matter. The carboxylic group on LA deprotonates in neutral conditions, but retains its proton during acidic conditions where Pt metal best oxidises LA. This could mean the OH of the carboxylic group may be desired in order to attract the molecule to the Pt surface. This allows the molecule to potentially adsorb to the catalyst surface for oxidation to take place.

A theory suggested for this oxidation reaction involved the formation of hydroxyl radicals at the surface of the Pt metal.[48] This is proposed through the following reaction:

$$H_2O \longrightarrow H^+ + e^- + \cdot OH \qquad (3\text{-}4)$$

The produced radicals are driven by the high potential formed at the electrode, which could be related to the oxidation of Pt on the electrode surface. The radical then oxidises LA in a two-step process as follows:

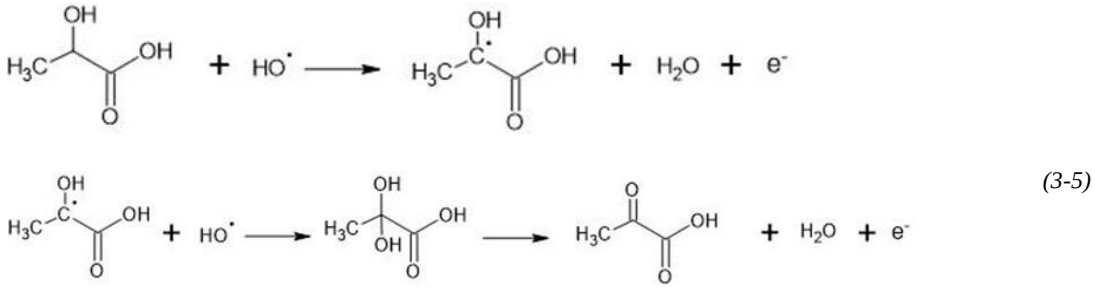

(3-5)

This reaction theoretically occurs on the surface of the Pt catalyst during acidic conditions. However, as LA deprotonates at neutral pH, this could be a reason why sensitivity for LA significantly decreases in PBS when using Pt as a catalyst on its own. It is possible that by combining Ni and Pt to form the mixed nanocomposite chains, synergistic effects may be achieved that can potentially enhance LA sensitivity. Theoretically, by combining metallic Pt and oxidised Ni, the following mechanism is proposed:

In addition to oxidising the secondary alcohol on LA as shown in reaction 3-3, Ni^{3+} may also oxidise the deprotonated carboxyl group of LA:

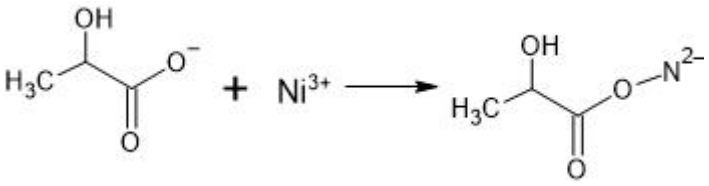

(3-6)

Highly reactive Ni^{3+} has demonstrated the ability to bind to carboxylic groups, which in turn brings the molecule to the surface which can potentially make it easier to adsorb to the Pt metal allowing for reaction 3-5 to proceed.[49] More research however needs to be conducted in order to confirm such theory.

Chapter 4: Conclusions and Future Work

Using AuNP Nanocomposite Chains For LA Detection Summary and Conclusions

The primary objective of using non-enzymatic materials such as metals and/or metal oxides to detect LA in isotonic pH conditions was achieved. It was found that by combining metallic Pt and oxidised Ni, real-time LA detection can be achieved in isotonic pH levels with good linearity. This was however done in a controlled environment using PBS buffer, and results may differ in real-life biological applications. More tests and data need to be collected and optimized to take the technology readiness level (TRL) to the next stage in order to incorporate such a sensor into NERv's platform. An adequate understanding of the hysteresis behaviour is also needed to enhance sensor accuracy. Bad hysteresis can affect real-life performance drastically, however there are models that have shown the ability help mitigate this once hysteresis behaviour is well-understood.[50] It should also be mentioned that the use of 2X PBS buffer, although used to decrease pH changes, contains an abundance of chloride ions which may interfere with sensor performance as other samples have shown a higher sensitivity using 1X PBS. Sensor specificity was also an area that was touched upon briefly. Although it initially presented good promise, in a real biological setting, there is bound to be a greater number of molecules that can potentially interfere with the system. In summary, this is still a step forward towards the primary objective, however future work is still required to take this sensor to market.

Future Work and Optimization

Enhancing sensor sensitivity is a key parameter as it directly correlates to better performance detecting LA and would also improve the limit of detection. To achieve this, several aspects need to be studied. As shown, the combination of materials may bring about synergistic

effects, and future work testing the addition of another co-catalyst may improve sensor performance. During the duration of this thesis, a tri-metallic nanocomposite comprising of Ni, Pt and V was tested for LA detection, but no noticeable enhancements were observed. However, that does not mean such is the case using other metals and metal oxides of other common catalysts such as Co, Fe, Cu and Ru, as combining materials can enhance both sensitivity and specificity in certain applicaitons.[51] Other combinations of materials in varying ratios should therefore be tested for LA sensitivity.

As previously mentioned, more work also needs to be done to determine the extent of our material's specificity and whether other molecules can interfere with the system. It is important to research and understand specificity to push the TRL of the LA sensor. Understanding specificity would determine whether a selective coating is required, or if a change in sensing material and/or measurement potential/method is the solution.[52] The proposed reaction mechanism is theoretical, and a further understanding of this mechanism would also enable us to understand how to further optimize both sensitivity and specificity, hence more work should be pursued in that regard. Understanding how the system works would enable us to better understand what happens when LA concentration decreases and how this affects settling time. Although models exist that can be used to overcome slow sensor recovery as observed in some of our data, a better understanding of the reaction dynamics can allow us to modify how certain tests are conducted or parameters measured.[53] Understanding the electrochemical reactions could also potentially help lead to solutions that could lower the measuring potential of the sensor, so that it uses less energy and creates lesser side reactions.

As the sensor is intended to be used for continuous monitoring, another parameter that should be investigated is temporal drift, which is how the sensor's response shifts over time. It is

important to distinguish whether temporal drift is present and to quantify it to determine if it is significant enough to warrant intervention. Such interventions can include electrode and electrochemical improvements, or modelling methods such as machine learning to mitigate the problem.[54]

The final steps needed to push the TRL of a product to market readiness are usually the hardest. More design work needs to be conducted to integrate a functioning sensor into NERv's platform. This includes sensor fabrication including suitable reference and working electrodes, as well as integrated circuits that can utilise the sensor. Work also needs to be conducted to determine suitable sensor shelf-life as well as stability in biological conditions and whether a biofouling coating is required to prevent interference from biological material.[55]

Although the first step has been taken, it is good practice to study and identify potential roadblocks ahead to find methods of overcoming them beforehand. This thesis demonstrated a potential nanocomposite as a non-enzymatic alternative to LA detection, but it should also be understood that there is still more work to come, and this is achieved through small achievements in research.

References

1 Pinto, A.; Faiz, O.; Bicknell, C.; Vincent, C. Acute traumatic stress among surgeons after major surgical complications. *Am. J. Surgery*. **2014**, 208 (4), 642–647.

2 Tevis, S. E.; Cobian, A. G.; Truong, H. P.; Craven, M. W.; Kennedy, G. D. Implications of Multiple Complications on the Postoperative Recovery of General Surgery Patients. *Annals of Surgery.* **2016**, 263 (6), 1213–1218.

3 Dencker, E. E.; Bonde, A.; Troelsen, A.; Varadarajan, K. M.; Sillesen, M. Postoperative complications: an observational study of trends in the United States from 2012 to 2018. *BMC Surgery.* **2021**, 21, 393.

4 Turrentene, F. E.; Denlinger, C. E.; Simpson, V. B.; Garwood, R. A.; Guerlain, S.; Agrawal, A.; Friel, C. M.; LaPar, D. J.; Stukenborg, G. J.; Jones, R. S. Morbidity, Mortality, Cost, and Survival Estimates of Gastrointestinal Anastomotic Leaks. J. of the *Am. Col Surg*. **2015,** 220 (2), 195-206.

5 Platell, C. The incidence of anastomotic leaks in patients undergoing colorectal surgery. *Col. Disease.* **2007**, 9 (1), 71-9.

6 Welsch, T.; von Frankenberg, M.; Schmidt, J.; Büchler, M. W. Diagnostik und Definition der Nahtinsuffizienz aus chirurgischer Sicht [Diagnosis and definition of anastomotic leakage from the surgeon's perspective]. *Der Chirurg; Zeitschrift fur alle Gebiete der operativen Medizen*, **2011,** 82 (1), 48–55.

7 Hyman, N.; Manchester, T. L.; Osler, T.; Burns, B.; Cataldo, P. A. Anastomotic Leaks After Intestinal Anastomosis. *Annals of Surgery*. **2007**, 245 (2), 254–258.

8 Moon, S. W.; Kim, J. J.; Cho, D. G.; Park, J. K. Early detection of complications: anastomotic leakage. *J. of Thoracic Disease.* **2019,** 11 (S5), S805–S811.

9 Molinari, E.; Giuliani, T.; Andrianello, S.; Talamini, A.; Tollini, F.; Tedesco, P.; Pirani, P.; Panzeri, F.; Sandrini, R.; Remo, A.; Laterza, E. Drain fluid's pH predicts anastomotic leak in colorectal surgery: results of a prospective analysis of 173 patients. *Minerva chirurgica.* **2020,** 75(1), 30–36.

10 Scott C. (2005). Misconceptions about Aerobic and Anaerobic Energy Expenditure. *J. of Int. S. of Sports Nutrition.* **2005,** 2 (2), 32–37.

11 Kintu-Luwaga, R.; Galukande, M.; Owori, F. N. Serum lactate and phosphate as biomarkers of intestinal ischemia in a Ugandan tertiary hospital: a cross-sectional study. *Int. Journal of Emergency Med.* **2013,** 6 (1).

12 Bini, R.; Ferrari, G.; Aprà, F.; Viora, T.; Leli, R.; Cotogni, P. Peritoneal lactate as a potential biomarker for predicting the need for reintervention after abdominal surgery. *J. of Trauma and Acute Care Surgery.* **2014,** 77 (2), 376–380.

13 Kovac, N.; Siranovic, M.; Peric, M. Relavance of peritoneal drainage fluid lactate level in patients with intra-abdominal hypertension. *Cogent Medicine.* **2017,** 4 (1).

14 Onor, M.; Gufoni, S.; Lomonaco, T.; Ghimenti, S.; Salvo, P.; Sorrentino, F.; Bramanti, E. Potentiometric sensor for non invasive lactate determination in human sweat. *Analytica Chimica Acta.* **2017,** 989, 80–87.

15 Zaryanov, N. V.; Nikitina, V. N.; Karpova, E. V.; Karyakina, E. E.; Karyakin, A. A. Nonenzymatic Sensor for Lactate Detection in Human Sweat. *Anal. Chem.* **2017,** 89 (21), 11198–11202.

16 Latson, K. M.; Nieto, J. E.; Beldomenico, P. M.; Snyder, J. R. Evaluation of peritoneal fluid lactate as a marker of intestinal ischaemia in equine colic. *Equine Vet. J.* **2010,** 37 (4), 342–346.

17 Tennent-Brown, B. S. Interpreting lactate measurement in critically ill horses: diagnosis, treatment, and prognosis. *Compendium.* **2012,** 34 (1), E2.

18 Park, R. Lactic acidosis. *Western j. of Med.* **1980,** 133 (5), 418–424.

19 Greenwald, D.; Nakamura, R.; diZerega, G. Determination of pH and pKa in human peritoneal fluid. *Current surg.* **1988,** 45 (3), 217–218.

20 Rathee, K.; Dhull, V.; Dhull, R.; Singh, S. Biosensors based on electrochemical lactate detection: A comprehensive review. *Biochemistry and Biophysics Reports.* **2016,** 5, 35–54.

21 Romero, M. R.; Ahumada, F.; Garay, F.; Baruzzi, A. M. Amperometric Biosensor for Direct Blood Lactate Detection. *Anal. Chem.* **2010**, 82 (13), 5568–5572.

22 Yüce, M.; Kurt, H. How to Make Nanobiosensors: Surface Modification and Characterisation of Nanomaterials for Biosensing Applications. *RSC Adv.* **2017,** 7 (78), 49386–49403.

23 Sedenho, G. C.; Lee, P. T.; Toh, H. S.; Salter, C.; Johnston, C.; Stradiotto, N. R.; Compton, R. G. Nanoelectrocatalytic Oxidation of Lactic Acid Using Nickel Nanoparticles. *J. of Phys. Chem.* **2015,** 119 (12), 6896–6905.

24 Kim, S.; Kim, K.; Kim, H. J.; Lee, H. N.; Park, T. J.; Park, Y. M. Non-Enzymatic Electrochemical Lactate Sensing by NiO and Ni(OH)2 Electrodes: A Mechanistic Investigation. *Electrochimica Acta.* **2018,** 276, 240–246.

25 Sedenho, G. G. C.; Lee, P. T.; Toh, H. S.; Salter, C.; Johnston, C.; Stradiotto, N. R.; Compton, R. G. The Electro-Oxidation of Lactic Acid at Platinum Microparticles and Polycrystalline Platinum Electrode. *Int. J. of Electrochem. Sci.* **2016,** 11, 2166-2176.

26 Chung, D. Y.; Kim, H.; Chung, Y. H.; Lee, M. J.; Yoo, S. J.; Bokare, A. D.; Sung, Y. E. Inhibition of CO Poisoning on Pt Catalyst Coupled With the Reduction of Toxic Hexavalent Chromium in a Dual-Functional Fuel Cell. *Sci. Reports.* **2014,** 4 (1).

27 Pu, L.; Fan, H.; Maheshwari, V. Formation of Microns Long Thin Wire Networks With Controlled Spatial Distribution of Elements. *Catal. Sci. Technol.* **2020,** 10, 2020-2028.

28 Chansuvarn, W.; Tuntulani, T.; Imyim, A. Colorimetric Detection of Mercury(II) Based on Gold Nanoparticles, Fluorescent Gold Nanoclusters and Other Gold-Based Nanomaterials. *TrAC Trends Anal. Chem.* **2015,** 65, 83–96.

29 Bernard, P.; Stelmachowski, P.; Broś, P.; Makowski, W.; Kotarba, A. Demonstration of the Influence of Specific Surface Area on Reaction Rate in Heterogeneous Catalysis. *J. Chem. Ed.* **2021**, 98 (3), 935–940.

30 Zakharov, N. S.; Popova, A. N.; Zakharov, Y. A.; Pugachev, V. M.; Russakov, D. M. Transmission Electron Microscopy for Evaluating the Structural Parameters of Nanoparticles. *J. Phys.: Conf. Ser.* **2021,** 1749, 012011.

31 Wang, H.; Kou, X.; Zhang, J.; Li, J. (2008). Large Scale Synthesis and Characterization of Ni Nanoparticles by Solution Reduction Method. *Bull. Mater. Sci.* **2008**, 31 (1), 97–100.

32 Naresh, K. M.; Boddeti, G.; Nowduri, A. Green Synthesis and Characterization of Platinum Nanoparticles using Sapindus mukorossi Gaertn. Fruit Pericarp. *Asian J. Chem*. **2017,** 29 (11), 2541–2544.

33 Martinez, J. P.; Carter, E. A. Effects of the Aqueous Environment on the Stability and Chemistry of β-NiOOH Surfaces. *Chem Mat.* **2018**, 30 (15), 5205-5219.

34 Grosvenor, A. P.; Biesinger, M. C.; Smart, R. S.; McIntyre, N. S. New Interpretations of XPS Spectra of Nickel Metal and Oxides. *Surf. Sci.* **2006,** 600 (9), 1771–1779.

35 Biesinger, M. C.; Payne, B. P.; Grosvenor, A. P.; Lau, L. W. M.; Gerson, A. R.; Smart, R. S. Resolving Surface Chemical States in XPS Analysis of First Row Transition Metals, Oxides and Hydroxides: Cr, Mn, Fe, Co and Ni. *Appl. Surf. Sci.* **2011,** 257 (7), 2717–2730.

36 Guangyang, L.; Meng, L.; Xiaodong, H.; Tengfei, L.; Donghui, X. Application of Gold-Nanoparticle Colorimetric Sensing to Rapid Food Safety Screening. Sensors. *Sensors (Basel).* **2018,** 18 (12), 4166.

37 Peuckert, M.; Coenen, F. P.; Bonzel, H. P. (1984). XPS Study of the Electrochemical Surface Oxidation of Platinum in N H2SO4 Acid Electrolyte. *Electrochimica Acta.* **1984**, 29 (10), 1305–1314.

38 Caporali, S.; Muniz-Miranda, F.; Pedone, A.; Muniz-Miranda, M. SERS, XPS and DFT Study of Xanthine Adsorbed on Citrate-Stabilized Gold Nanoparticles. *Sensors.* **2019**, 19, 2700.

39 Ganesh, K.; Soumen, R.; Ravichandran, Y.; Janarthanan. Dynamic Approach to Predict pH Profiles of Biologically Relevant Buffers. *Biochemistry and Biophysics Reports*. **2017,** 9, 121–127.

40 Arulmozhi, N.; Esau, D.; Lamsal, R. P.; Beauchemin, D.; Jerkiewicz, G. Structural Transformation of Monocrystalline Platinum Electrodes upon Electro-oxidation and Electro-dissolution. *ACS Catal*. **2018,** 8 (7), 6426-6439.

41 Jacobse, L.; Vonk, V.; McCrum, I. T.; Seitz, C.; Koper, M. T. M.; Rost, M. J.; Stierle, A. Electrochemical Oxidation of Pt(111) Beyond the Place-Exchange Model. *Electrochimica Acta*. **2022**, 407, 139881.

42 Wang, C.; Chang, T.; Yang, H.; Cui, M. Surface Physiological Changes Induced by Lactic Acid on Pathogens in Consideration of pKa and pH. *Food Control*. **2014,** 46, 525–531.

43 Forootan, A.; Sjoback, R.; Bjorkman, J.; Sjogreen, B.; Linz. L.; Kubista, M. Methods to Determine Limit of Detection and Limit of Quantification in Quantitative Real-Time PCR (qPCR). *Biomol. Det. Quant.* **2017**, 12, 1-6.

44 Armbruster D. A.; Pry, T. Limit of Blank, Limit of Detection and Limit of Quantitation. *Clin. Biochem. Rev*. **2008,** 29 Suppl 1, S49-52.

45 Saadati, N.; Abdullah, M. P.; Zakaria, Z.; Sany, S. B. T.; Rezayi, M.; Hassonizadeh, H. Limit of Detection and Limit of Quantification Development Procedures for Organochlorine Pesticides Analysis in Water and Sediment Matrices. *Chem. Centl. J.* **2013,** 7(63).

46 Morris, K. A. What is Hysteresis? *App. Mech. Rev.* **2012,** 64 (5), 050801.

47 Medway, S. L.; Lucas, C. A.; Kowal, A.; Nichols, R. J.; Johnson, D. In Situ Studies of the Oxidation of Nickel Electrodes in Alkaline Solution. *J. Electronal. Chem.* **2006**, 587 (1), 172–181.

48 Horányi, G. On the Electrochemical Behaviour of Pyruvic and Lactic Acids at a Platinized Platinum Electrode in Acid Medium. *J. Electroanal. Chem. Interfacial Electrochem.* **1981**, 117(1), 131–137.

49 Pirovano, P.; Farquhar, E. R.; Swart, M.; McDonald, A. R. Tuning the Reactivity of Terminal Nickel(III)-Oxygen Adducts For C–H Bond Activation. *J. Am. Chem. Soc*. **2016,** 138 (43), 14362-14370.

50 Visone, C. Hysteresis Modelling and Compensation For Smart Sensors and Actuators. *J. Phys. Conf. Ser*. **2008,** 138, 012028.

51 Xiao, T.; Huang, J.; Wang, D.; Meng, T.; Yang, X. Au and Au-Based Nanomaterials: Synthesis and Recent Progress in Electrochemical Sensor Applications. *Talanta.* **2020**, 206, 120210.

52 Cesarino, I.; Hümmelgen, I. A. (2015). An Additional Tool Towards Overcoming Absence of Specificity of Carbon Nanostructure-Based Electrochemical Sensors—Application to Estriol and Estradiol Detection and Distinction. *J. Solid State Electrochem.* **2015,** 19 (10), 3045–3050.

53 Monroy, J. G.; González-Jiménez, J.; Blanco, J. L. Overcoming the Slow Recovery of MOX Gas Sensors through a System Modeling Approach. *Sensors*. **2012,** 12 (12), 13664–13680.

54 Sinha, S.; Bhardwaj, R.; Sahu, N.; Ahuja, H.; Sharma, R.; Mukhiya, R. Temperature and Temporal Drift Compensation For Al2O3-gate ISFET-based pH Sensor Using Machine Learning Techniques. *Microelectronics J.* **2020,** 97, 104710.

55 Timilsina, S. S.; Durr, N.; Yafia, M.; Sallum, H.; Jolly, P.; Ingber, D. E. Ultrarapid Method for Coating Electrochemical Sensors with Antifouling Conductive Nanomaterials Enables Highly Sensitive Multiplexed Detection in Whole Blood. *Adv. Healthc. Mater*. **2021**, e2102244.

Appendix

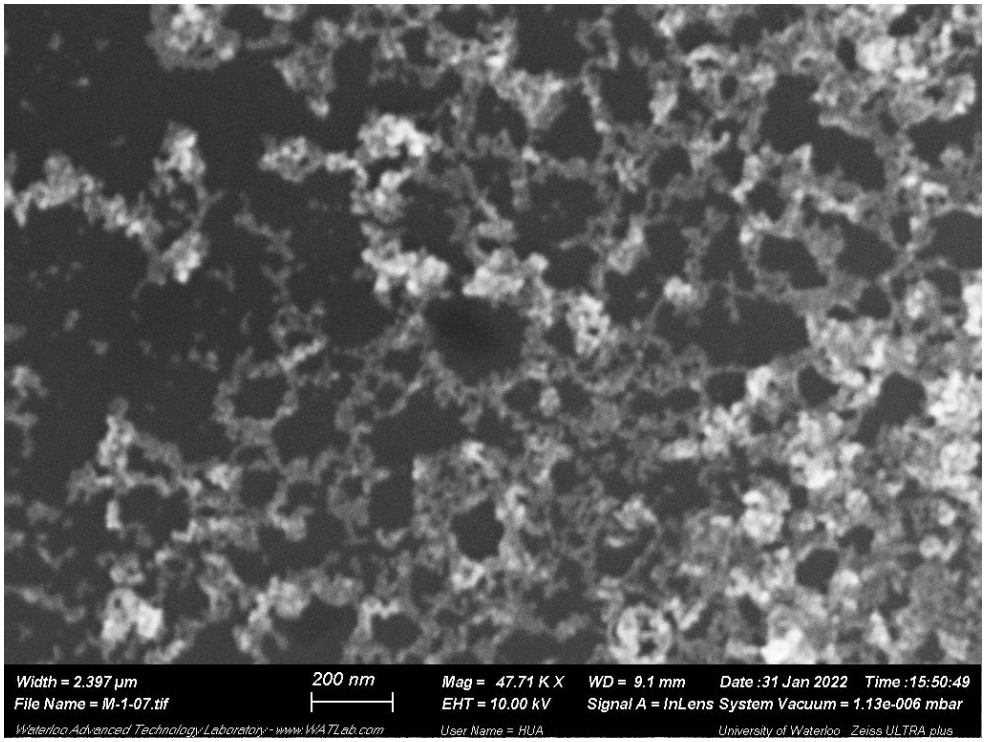

Figure S-1: SEM image of AuNP pre-assembled nanocomposite chains comprised of 1:10 Ni: Pt. SEM shows similar structure to 1:2 Ni:Pt nanocomposite.

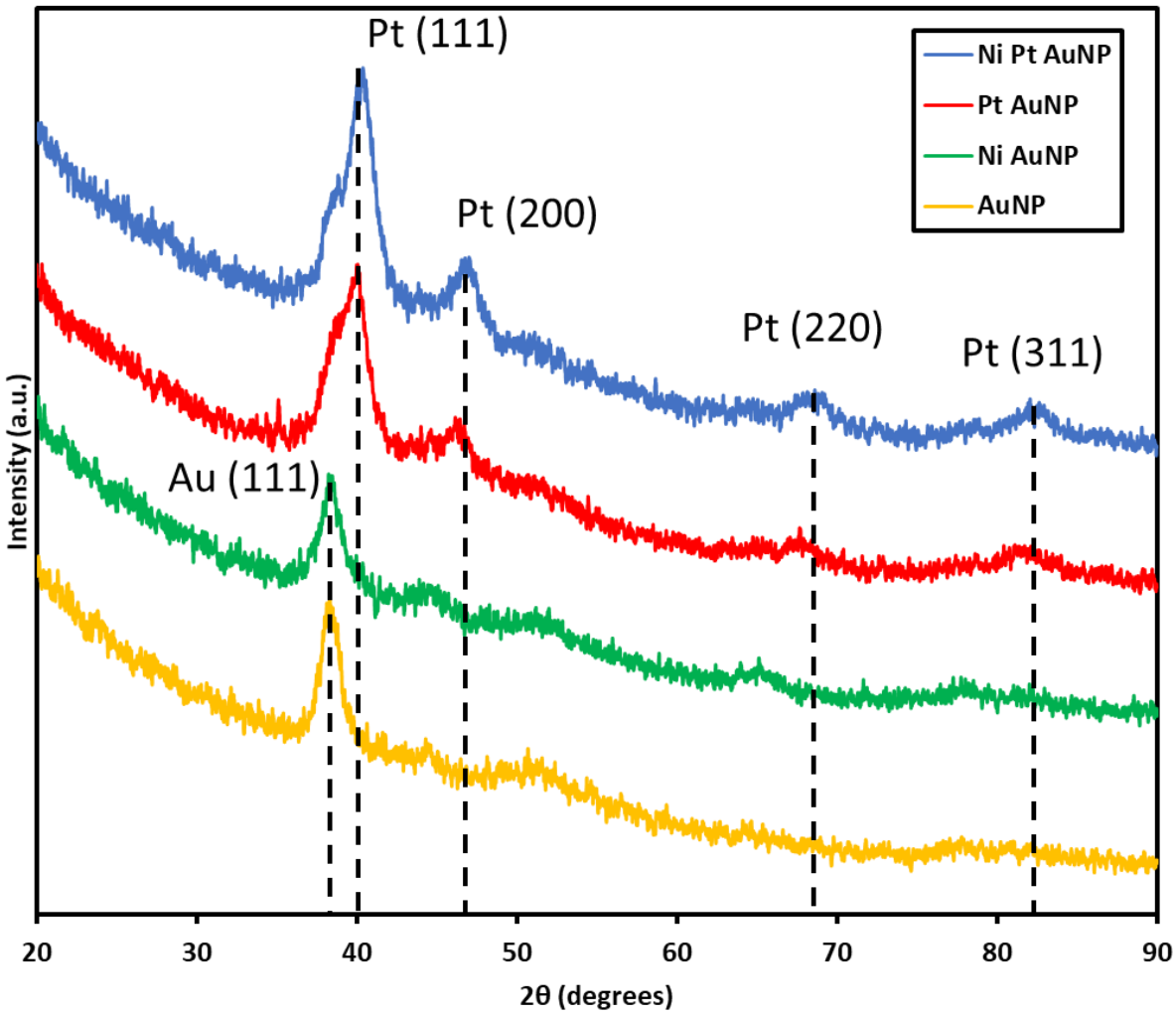

Figure S-2: XRD pattern of AuNPs, reduced Ni AuNPs, reduced Pt AuNPs, and reduced 1:3 Ni:Pt AuNP nanocomposite chains. Pt peaks are labelled as well as Au (111). Ni did not show peaks implying it is amorphous.